ANALYSIS OF TAPERED LAMINATED COMPOSITE TUBES UNDER TENSION AND TORSION

by

CHETHANA SHANKARA RAO

Presented to the Faculty of the Graduate School of

The University of Texas at Arlington in Partial Fulfillment

of the Requirements

for the Degree of

MASTER OF SCIENCE IN MECHANICAL ENGINEERING

THE UNIVERSITY OF TEXAS AT ARLINGTON

May 2007

ACKNOWLEDGMENTS

I would like to thank Dr. Chan for his patience and time, and his unlimited guidance and support, which made this thesis possible. I would also like to thank Dr. Lawrence and Dr. Nomura for serving on my thesis committee. I would also like to thank all the professors of the MAE department because of whom; my master's degree has been a huge success in terms of learning and knowledge acquisition.

I would also like to express my gratitude towards my parents, my beloved brother and my friends for their unending support and encouragement throughout my career, especially during my master's degree.

April 20th , 2007

ABSTRACT

ANALYSIS OF TAPERED LAMINATED COMPOSITE TUBES UNDER TENSION AND TORSION

Publication No. _____

Chethana Shankara Rao, M.S.

The University of Texas at Arlington, 2007

Supervising Professor: Wen S Chan

Closed form expressions for determining the displacement and twisting angle of tapered composite tubes are developed. The analytical expressions are developed based on the modified laminated plate theory which includes the tubular wall curvature of the laminate. It is found that the axial deformation and the twisting angle calculated by the current method agree well with the results obtained from the finite element method.

The effect of stacking sequence, taper angle and fiber orientations on the axial deformation and twisting angle are studied by using the developed method. It is found that the taper angle plays a significant role on the axial deformation and the twisting angle provided the laminate lay-up is given.

TABLE OF CONTENTS

LIST OF ILLUSTRATIONS

LIST OF TABLES

Table

CHAPTER 1

INTRODUCTION

1.1 Overview

The applications of composite materials in aeronautical and other engineering structures are ever increasing, due to their highly desirable properties like high specific strength/ stiffness, low co-efficient of expansion, damping properties and directional dependence. One of the first uses of composite materials was about 30 years ago in the empennage skins of F14 aircraft. With extensive research in the field, composite materials are now being applied to primary structures of many aircrafts including fuselage and wings. Of-late composites are gaining popularity in automobile and civil industries. Fiber reinforced plastics (FRP), which is one of the most widely used composite in automobile industry, contributes towards reduced fuel consumption, increased pay load, strength and stiffness and lesser corrosion.

Laminated composite shells in particular are prominent in bearing various types of loads and are hence used in many engineering structures. The analysis of laminated composites is quite complicated since the material behavior is anisotropic, which gets further intensified in the analysis of complex structures like shells. Laminated composite shells are used in fuselage structures, pressure vessels, missiles and spacecraft, jet nozzles etc. A shell is defined as a thin walled body with a curvature at least in one direction.

The use of thin walled tube constitutes the most unified approach for characterizing the mechanical properties of fiber reinforced composites. A thin walled tube, whose radius to thickness ratio is very large, is under a state of uniform stress under combined tension, torsion and internal pressure. Some applications of composite shells are described below.

Carbon fiber baseball bats (see *Fig 1.1*) are used in amateur baseball since the flying distance becomes longer and serves as a good replacement for wood, which is is becoming less and less available.

Fig 1.1 Composite baseball bat

Tennis rackets (*Fig 1.2*) made of carbon fibers are far lighter than wooden rackets and have higher service life than wooden rackets.

Fig 1.2 Composite tennis rackets

Golf shafts (*Fig 1.3*) made of composites are much lighter than metal shafts giving higher swing speed for a given power. Composite golf shafts, which were used initially only by senior players and ladies is now gaining popularity among professional and amateur players.

Fig 1.3 Composite golf shaft

Composites are used in compressed natural gas (CNG) tanks (*Fig 1.4*) for natural gas cars due to their light weight.

Fig 1.4 Composite CNG tank

Other applications include wind mill blades, rollers, shafts and X ray inspection equipment. Laminated cylindrical shells are used in pressure vessels, missiles and aircraft, fuselage structures etc. Laminated conical shells are often used as transition elements between cylinders of different diameters, end closures etc. The use of laminated composites in conical shells are however limited to tubes of low radius ratio, since high radius ratios results in a non-uniform orientation of fibers in a ply.

1.2 Literature Survey

Good research has been carried out in the past; many of which focus on the behavior of laminated shells under different loading conditions, hygrothermal effects etc. Other studies in the area include buckling and post buckling analysis of laminated shells, delaminations and thermal analysis. Many of these studies have been carried out using finite element technique.

Reddy [1] gives a detailed description of the analysis of laminated plates in vibration; buckling and bending using the Classical Laminated Plate theory and First order shear deformation theory. He also discusses the vibration and buckling phenomenon of cross ply laminated circular cylindrical shells.

Much focus has not been poured on the analytical modeling of laminated shells. While finite element techniques are cumbersome and time consuming, experimental techniques need proper specimens and mounting techniques. In such conditions, there is a high need for an easy-to-use analytical solution. Demirhan and Chan [2] have presented two analytical closed form expressions for the evaluation of the stiffness matrices of cylindrical composite tube, one employing the laminated plate theory and the other employing the laminated shell theory. The models are compared with the smear property approach and also with the results from a finite element model. In their model, effect of curvature of the laminate in tubes are included Recently, Lin and Chan [3] modified the former model for circular tube to develop a model for elliptical cylindrical tube under bending. Finite element model is used for the verification of this model.

Ren [4] has developed and elastic solution for an anisotropic laminated circular cylindrical shell simply supported and subjected to axisymmetric loads using three dimensional elasticity theory. Many research has been conducted on laminated shells using numerical techniques like finite element method. Tafreshi [5] has presented a computational model for the delamination in isotropic and laminated composite cylindrical shells. A combined double layer and single layer of shell elements are

employed to study the effects of delamination on the global load carrying capacity of such systems under axial compressive load. Vaziri [6] has studied the sensitivity of buckling behavior of cracked composite cylindrical shells to service life buckling by performing a linear buckling analysis. Computational models are developed by using a special meshing technique in which the element size is reduced incrementally from the uncracked region to the cracked tip. Gummadi and Palazotto [8] have presented a progressive failure analysis on cylindrical shells. Non linear finite element formulation with large rotation capability is used to predict the onset of failure modes. The different failure modes considered are: fiber breakage, matrix cracking and delamination.

Yan, Ying and Chen [7] have studied the behavior of simply supported laminated cylindrical shell with viscoelastic interfaces in cylindrical bending.

Very little work has been carried out in the field of laminated conical shells. Most of them deal with buckling and vibration, some of which are presented below.

Correia, Soares and Herskovits [9] have presented a numerical method for the structural analysis of laminated conical shells using a quadrilateral isoparametric element based on higher order shear deformation theory. The model developed can be used to perform static analysis with arbitrary boundary conditions and loads and for solving eigen values problems.

Liu [10] has developed a theory for non linear bending of symmetrically laminated, cylindrically orthotropic, shallow conical shells subjected to an

axisymmetrically distributed load. Transverse shear effects were also included in his model.

Goldfield [11] has studied the sensitivity of stiffened conical shells to imperfection via post buckling analysis.

Raju, Chandra and Rao [12] have presented the transient temperatures in laminated composite conical shells subjected to aerodynamic heating. Unsteady heat conduction equations for a laminated composite conical shell corresponding to an axisymmetric temperature field are formulated.

Most of the research in laminated conical shells is based on thermal and buckling analysis. No attempt has been made in the past to study the structural response of laminated conical shells (tapered composite tubes).

1.3 Objective and Approach of Thesis

In the current research, an effort is made to develop an analytical model for the computation of deformations of tapered laminated composite tube under axial tension and torsion. IM6/ 3501-6 Graphite/ Epoxy is used as the composite material in the current research. The analytical models are developed based on the laminated plate theory and are extensions of the model developed for circular cylindrical tubes [3], which is discussed in detail in Chapter 2. The analytical model developed is more like a procedure than a closed form solution. The models are validated using a finite element model,

which is first used to analyze an isotropic tube in order to ensure the validity of the model. The finite element model is developed in the computer program ANSYS. Parametric studies are conducted on tubes to study the effect of stacking sequence, fiber orientation and taper angles.

1.4 Outline of the Thesis

A review on circular cylindrical tubes [2] is carried out in Chapter 2. Analytical solution and finite element model for tapered tubes (Isotropic and composite) under axial tension are discussed in Chapter 3. Chapter 4 deals with analytical model and finite element model of tapered tubes (Isotropic and Composite) under torsion. Parametric studies to study the effects of stacking sequence, fiber orientation and taper angles are discussed in Chapter 5. Finally conclusions and recommendations are presented in Chapter 6. MATHEMATICA codes and ANSYS batch files are presented in the Appendix section.

CHAPTER 2

STIFFNESS MATRICES OF UNIFORM CIRCULAR TUBES

Chan and Demirhan [2] developed two new analytical methods for evaluating the stiffness matrices of laminated uniform circular tubes. The two methods laminated plate approach and laminated shell approach account for the stacking sequence and curvatures. The laminated shell approach is however not relevant, hence not discussed here. Both the theories are developed based on the lamination theory.

2.1 Geometry of the Tube

The laminated tube considered is a uniform tube, with circular cross section with an outer radius R_o, inner radius R_i and a length L. The length of the tube is sufficiently larger than its radii. Hence the tube considered is a long tube. In all the derivations the basic assumption of 'Plane remains plane after deformation' is made.

2.2 Stiffness Matrices of the Tube

The current model called the laminated plate theory is based on the conventional lamination theory. According to the lamination theory the stiffness matrices of an $n\ ply$ laminate with a ply thickness t_{ply} are given by:

$$[A] = \sum_{k=1}^{n} \left[\overline{Q}\right]_k \left(h_k - h_{k-1}\right)$$

$$[B] = \frac{1}{2} \sum_{k=1}^{n} \left[\overline{Q}\right]_k \left(h_k^2 - h_{k-1}^2\right) \tag{2.1}$$

$$[D] = \frac{1}{3} \sum_{k=1}^{n} \left[\overline{Q}\right]_k \left(h_k^3 - h_{k-1}^3\right)$$

where $\left[\overline{Q}\right]_k$ is the reduced stiffness matrix of the k^{th} layer. In the above form, the $\left[\overline{Q}\right]_k$ matrices have transformation matrices in the z direction only, which accounts for the fiber orientation. In the current research, along with a transformation about z, we also have to include a transformation about the x direction, which is discussed later in the chapter.

In order to develop the model, an infinitesimal plate element of the tube is considered as shown in the *Fig. 2.1*. The infinitesimal element is inclined at an angle θ to the z' axis of the tube. In order to develop the model, reduced stiffness matrices of the plies, which accounts for the fiber orientation are evaluated.

$$\left[Q^{'}\right] = \left[T_{\sigma}\left(-\alpha\right)\right]_z \cdot [Q] \cdot \left[T_{\varepsilon}\left(+\alpha\right)\right]_z$$

The element which is inclined at an angle θ with the z' axis is rotated about x' axis to make it parallel to y' axis. Hence the reduced stiffness matrix, $\left[Q'\right]$ of the individual plies needs to be transformed about the x axis. As we know, the transformation

of a reduced stiffness matrix, has both stress and strain transformation matrices, $[T]_\sigma$ and $[T]_\varepsilon$. These matrices are obtained as described below.

Since, the infinitesimal element is 2 dimensional, we can get the stress transformation matrix $[T]_\sigma$ for a $2D$ case by striking off the 2, 3 and 4th rows and columns of the 3 dimensional $[T_\sigma]_x$ matrix.

$$\text{Thus, } [T_\sigma]_x = \begin{bmatrix} 1 & 0 & 0 \\ 0 & m^2 & 0 \\ 0 & 0 & m \end{bmatrix} \tag{2.2}$$

Similarly we can find that the strain transformation matrix, $[T]_\varepsilon$ is equal to the stress transformation matrix $[T]_\sigma$. Hence,

$$[T_\varepsilon]_x = \begin{bmatrix} 1 & 0 & 0 \\ 0 & m^2 & 0 \\ 0 & 0 & m \end{bmatrix}$$

We can also note that, since the transformation matrices contain only m, the *cosine* terms, the matrices are the same for $+\theta$ or $-\theta$ terms. Hence, reduced stiffness matrix after x rotation will be given by:

$$\left[\overline{Q}\right] = [T_\sigma]_x \left[Q'\right][T_\varepsilon]_x \tag{2.3}$$

The stiffness matrices, $[A]$, $[B]$ and $[D]$ are then calculated using the lamination theory:

$$
\begin{aligned}
[A] &= \sum_{k=1}^{n} \left[\overline{Q}\right]_k (h_k - h_{k-1}) \\
[B] &= \frac{1}{2} \sum_{k=1}^{n} \left[\overline{Q}\right]_k (h_k^2 - h_{k-1}^2) \\
[D] &= \frac{1}{3} \sum_{k=1}^{n} \left[\overline{Q}\right]_k (h_k^3 - h_{k-1}^3)
\end{aligned}
\tag{2.4}
$$

The above matrices need to be translated to the y' axis using the parallel axis theorem. Here, $z = R\,Cos\theta$. Hence, the new stiffness matrices are given by:

$$
\begin{aligned}
\left[A'\right] &= [A] \\
\left[B'\right] &= [B] + R\,Cos\theta\ [A] \\
\left[D'\right] &= [D] + 2R\,Cos\theta\ [B] + \left(R\,Cos\theta\right)^2 [A]
\end{aligned}
\tag{2.5}
$$

Note that the stiffness matrices are in terms of R , where R is the mid-thickness radius of the circular tube, $R = R_0 - \frac{n}{2} t_{ply}$.

These matrices are then integrated over the entire θ domain to evaluate the stiffness matrices of the tube at the section.

$$
\begin{aligned}
\left[\overline{A}\right] &= R \int_0^{2\pi} \left[A'\right]\, d\theta \\
\left[\overline{B}\right] &= R \int_0^{2\pi} \left[B'\right]\, d\theta \\
\left[\overline{D}\right] &= R \int_0^{2\pi} \left[D'\right]\, d\theta
\end{aligned}
\tag{2.6}
$$

Note that R is not a function of θ and is hence taken out of the integration.

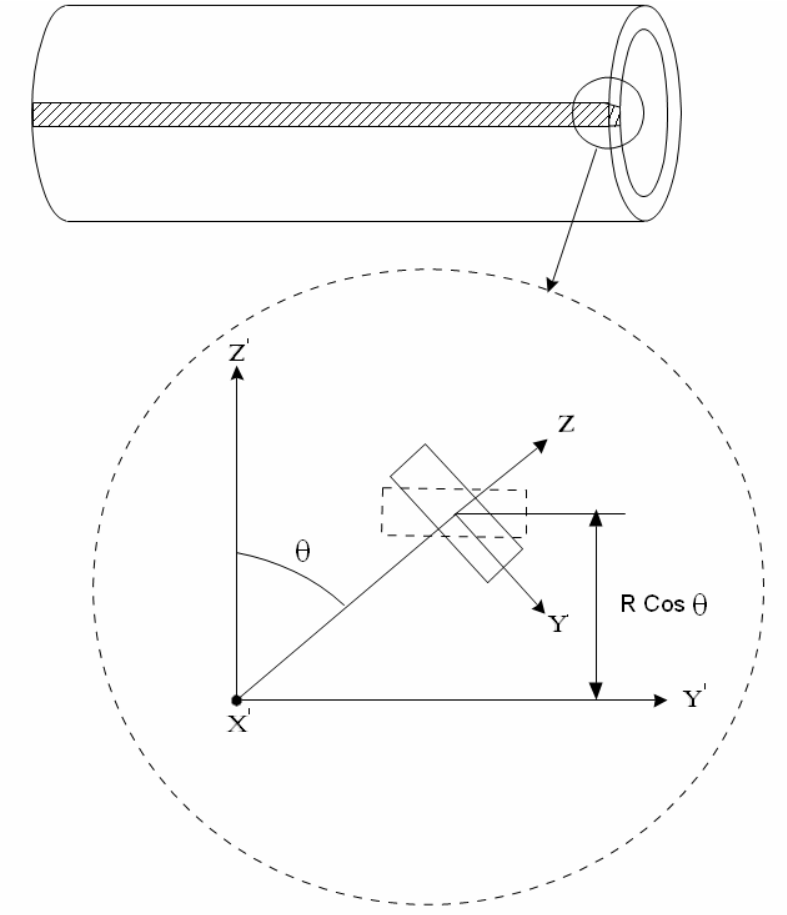

Fig 2.1 Development of Analytic Solution using Laminated Plate Theory

The above matrices can be expanded as:

$$\left[\bar{A}\right] = R\int_0^{2\pi}\left[A\right]\ d\theta$$

$$\left[\bar{B}\right] = R\int_0^{2\pi}\left[B\right]\ d\theta + R^2\int_0^{2\pi}\left[A\right]Cos\theta\, d\theta \qquad (2.7)$$

$$\left[\bar{D}\right] = R\int_0^{2\pi}\left[D\right]\ d\theta + 2R^2\int_0^{2\pi}\left[B\right]Cos\theta\, d\theta + R^3\int_0^{2\pi}\left[A\right]Cos^2\theta\, d\theta$$

2.3 Axial Stiffness

The relationship between forces and moments on the tube and the mid-plane strains and curvatures are given by:

$$\begin{bmatrix} N \\ M \end{bmatrix} = \begin{bmatrix} \bar{A} & \bar{B} \\ \bar{B} & \bar{D} \end{bmatrix} \cdot \begin{bmatrix} \varepsilon_o \\ \kappa \end{bmatrix}$$

$$\begin{bmatrix} \varepsilon_o \\ \kappa \end{bmatrix} = \begin{bmatrix} \bar{a} & \bar{b} \\ \bar{b}^T & \bar{d} \end{bmatrix} \cdot \begin{bmatrix} N \\ M \end{bmatrix} \tag{2.8}$$

ε_o and κ are the mid-plane strains and curvatures.

For an axial tensile case, N_x is the only applied load. Hence, the mid-plane axial deformation ε_o^x is given by:

$$\varepsilon_o^x = \bar{a}_{11} \cdot N_x \tag{2.9}$$

Hence, the axial stiffness will be given by $\frac{1}{\bar{a}_{11}}$

2.4 Torsional Stiffness

For a torsion case, only a moment M_{xy} (torque T) is applied. Hence the mid-plane angle of twist κ_{xy} will be given by,

$$\kappa_{xy} = \bar{d}_{66} \cdot M_{xy} \tag{2.10}$$

Hence the torsional stiffness is given by $\frac{1}{\bar{d}_{66}}$

2.5 Smeared Property Approach

This approach is more often used for the calculation of extensional and bending stiffness of the tube. The equivalent or smeared moduli of the walled laminate of the tube is used. The stiffness of the tube is then calculated using the conventional formula that is commonly used for isotropic tubes as shown below.

$$\text{Axial Stiffness } E_x A = E_x \cdot \pi \left(R_o^2 - R_i^2 \right) \tag{2.11}$$

$$\text{Bending Stiffness } E_x I = E_x \cdot \frac{\pi}{4} \left(R_o^4 - R_i^4 \right)$$

E_x is the equivalent modulus of the tube in the x direction.

2.6 Bending Stiffness Comparison between the Approaches

In Ref [2], Chan and Demirhan calculated the bending stiffness of a composite tube and compared their results with the smear property approach as well as the finite element method, The model is also confirmed by experimental results [19].

CHAPTER 3

TAPERED TUBES UNDER AXIAL TENSION

3.1 Analytical Solution for an Isotropic Tube

Consider a uniform thickness tapered tube with a mid-thickness larger radius R_L and a mid-thickness smaller radius R_S , where t is the thickness of the tube as shown in *Fig 3.1*. Let L be the length of the tube.

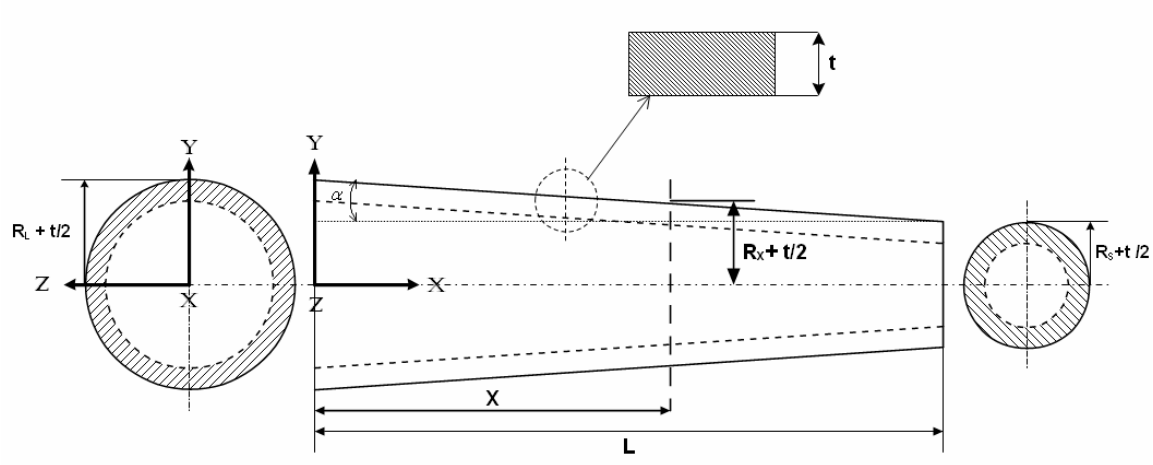

Fig 3.1 Dimensions of the Tapered Tube

The area of the larger end of the tapered tube will be:

$$A_L = \pi\left[\left(R_L + \frac{t}{2}\right)^2 - \left(R_L - \frac{t}{2}\right)^2\right] \qquad (3.1)$$

$$A_L = 2\pi R_L t$$

Similarly, the area at the smaller end of the tube will be given by:

$$A_S = 2\pi R_S t \tag{3.2}$$

The mid-thickness radius of the tapered tube at a distance x from the larger end, R_x will be given by:

$$R_x = R_L - x\tan\alpha \tag{3.3}$$

Where α is the taper angle of the tube and $tan\alpha = \frac{\Delta R}{L}$; ΔR is the difference between the large and small radii of the tube;

$$\Delta R = R_L - R_S$$

Hence, the area of the section of the tube at a distance x is given by:

$$\begin{aligned} A_x &= 2\pi R_x t \\ A_x &= 2\pi t[R_L - x\tan\alpha] \end{aligned} \tag{3.4}$$

We know, the deformation of the tapered tube at a distance x, subjected to an axial force F will be,

$$\begin{aligned} \delta_x &= \int_0^x \frac{Fdx}{EA_x} \\ &= \int_0^x \frac{Fdx}{2\pi Et\left(R_L - x\tan\alpha\right)} \\ &= \frac{F}{2\pi Et}\int_0^x \frac{dx}{\left(R_L - x\tan\alpha\right)} \end{aligned} \tag{3.5}$$

The axial deformation of the tapered bar δ_x at any section, distance x from the fixed end, will be hence given by:

$$\delta_x = \frac{F}{2\pi E\, t\, \tan\alpha} \ln\left(\frac{R_L}{\left(R_L - x\tan\alpha\right)}\right) \tag{3.6}$$

For a limiting case of a cylindrical tube, where $\alpha = 0$ the deformation can be found as:

$$\lim_{\alpha\to 0}\delta_x = \lim_{\alpha\to 0}\left(\frac{F}{2\pi E\, t\, \tan\alpha} \ln\left(\frac{R_L}{\left(R_L - x\tan\alpha\right)}\right)\right) \tag{3.7}$$

Using L' Hospitale's rule, we can find out for an axial case,

$$\delta_x = \frac{Fx}{2\,\pi\, E\, t\, R_L} \tag{3.8}$$

The above equation can be verified from a solid mechanics text book.

3.2 Finite Element Model of an Isotropic Tube

3.2.1 Geometry and Modeling

A model of a tapered tube with dimensions R_{LI} = 0.75 in, R_{SI} = 0.25 in, and a total thickness $t\,(6\,t_{ply})$ = 0.03 in is created using ANSYS. R_{LI} is the inner larger radius and R_{SI} is the inner smaller radius of the tube.

Refer to *Fig 3.2.* Key points $11\,(0, R_{LI})$, $12\,(L, R_{SI})$, $21\,(L, R_S + t_{ply})$, $22\,(0, R_L + t_{ply})$, are created using K command on ANSYS. Areas are created using these key points using the A command. In a similar fashion, 6 areas are created by incrementing the y co-ordinate by t_{ply}. These areas are then swept about a longitudinal

axis to create volumes using the VROTAT command. The VROTAT command necessitates that at least 2 volumes be created along the circumference. Thus a model of the tube, consisting of 12 volumes is created.

AL 2024/T3 with properties, E = 1.0498e7 and ν = 0.33 is used as the material of the tube.

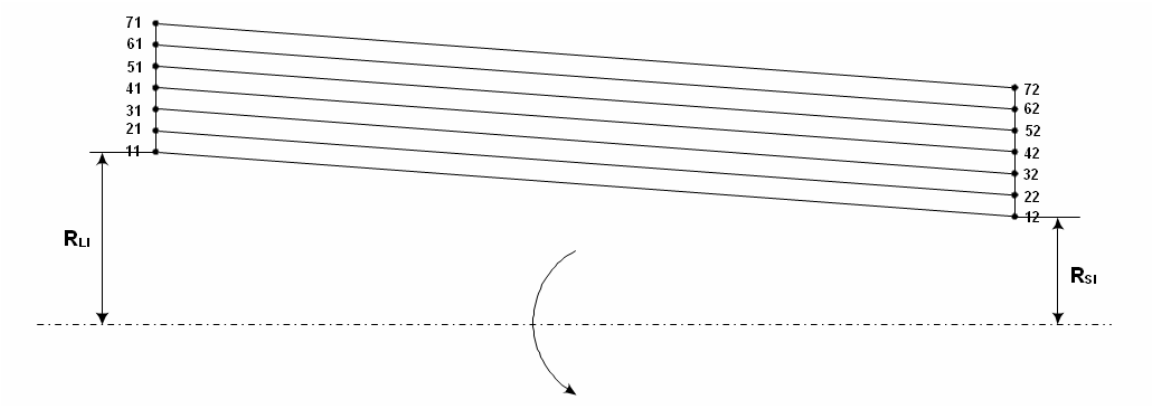

Fig 3.2 Development of the Finite Element Model

3.2.2 Development of the Model

To establish the correct mesh size, the model has to be checked for convergence of results. The convergence test for the tapered tube is carried out as follows. A model of an isotropic (Al 2024/T3) tapered tube with a geometry discussed in Section 3.2.1 is created. The element, SOLID 95, which has 20 nodes with 3 translational degrees of freedom (UX, UY and UZ) at each node is used for meshing the model. The mesh size is varied from 720 to 9000 elements and an axial force of 500 lb is applied on the tube. The mesh size of the lines in the thickness direction is maintained constant, and is equal to 1 element per line. The mesh sizes of the lines along the length and along the

circumference are varied. The axial deformation *UX* of the tube is noted for each mesh size and are tabulated in *Table 3.1*

Table 3.1 Table showing the convergence of results with increase in the number of elements

No. of Elements along Thickness	No. of Elements along Length	No. of Elements along Circumference	Total No. of elements	UX from Finite Element Method (*in*)
6	10	12	720	2.990E-03
6	20	20	2400	3.002E-03
6	30	24	4320	3.007E-03
6	40	24	5760	3.010E-03
6	50	30	9000	3.010E-03

Fig 3.3 shows the graph of axial deformation versus the number of elements in the model. From the plot, it can be seen that the results start converging at 5760 elements. A mesh size of 9000 elements with 50 elements per length, 30 per circumference is adopted in development of the model.

3.2.3 Boundary Conditions:

Fig 3.4 shows a model of the tapered tube with the boundary conditions. A MASS21 element is created at the master node (2) located at the center of the smaller end of the tube. Using CERIG command, a rigid region is created at the smaller end of the tube in order to ensure uniform displacement in a section. At the larger end, all the nodes are fixed in the (x) direction. A force FX of 500 lb is applied on the master node in the axial (x) direction.

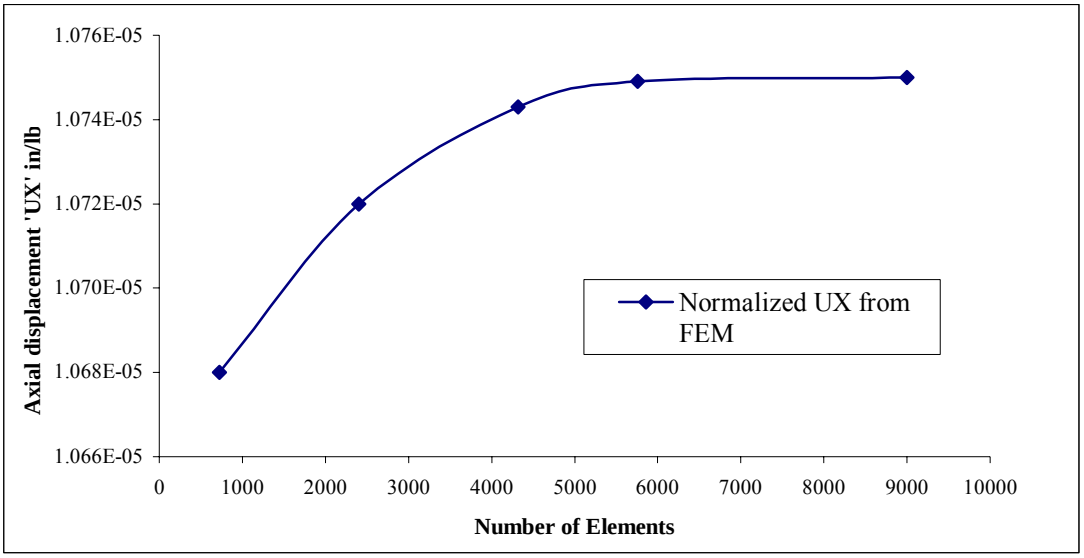

Fig 3.3 Convergence Plot

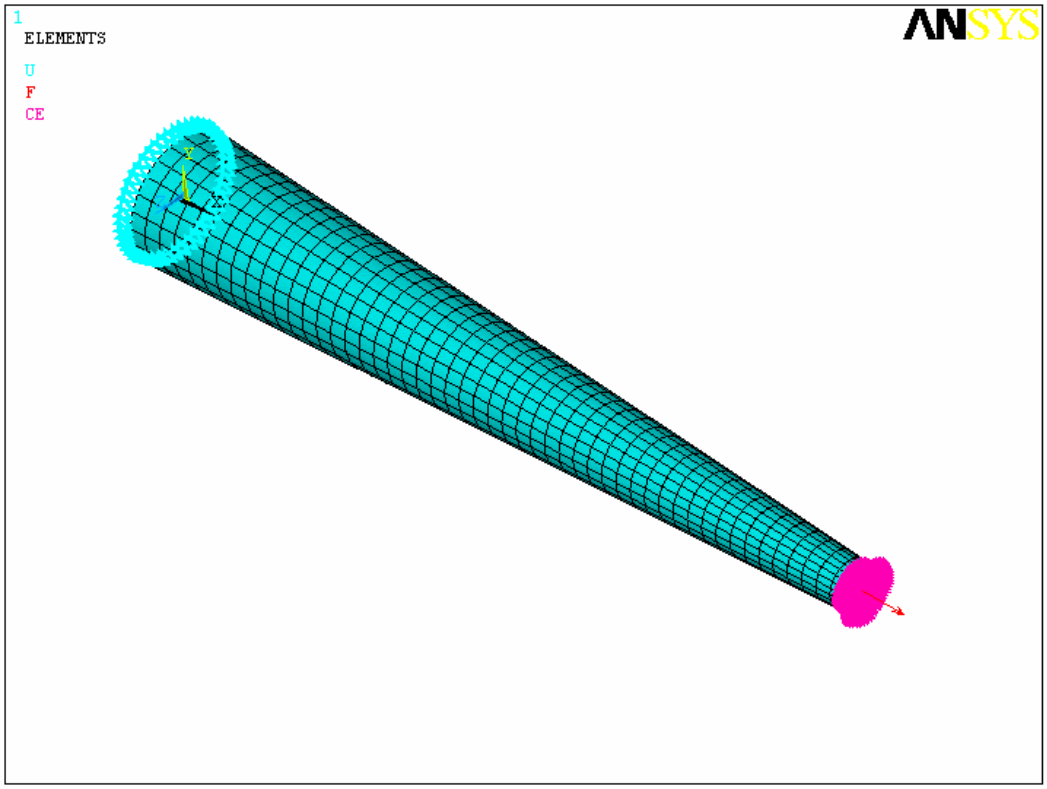

Fig 3.4 Finite Element Model of an Isotopic Tube with Boundary Conditions

3.3 Results Comparison

Table 3.2 shows the comparison of the results between the analytic solution and the finite element method. The percentage difference was calculated using the percent value of the ratio of the difference between the analytical and FEM results to the FEM value. *Fig 3.5* shows the graph of displacement of the tube in x direction, '*UX* ' with respect to the distance from fixed end 'x'. It can be observed from the graph that the analytic solution is in excellent agreement with the finite element results. Thus the finite element model developed can make a good ground for comparison of the analytical model and hence can be used for modeling the composite tube.

Table 3.2 Comparison of normalized axial deformation from analytical method and finite element method

Distance from fixed end x (in)	Normalized Analytical Solution (in/lb)	Normalized FEM Solution (in/lb)	% Difference
1	6.83E-07	7.00E-07	2.58
2	1.41E-06	1.44E-06	1.55
3	2.20E-06	2.23E-06	1.17
4	3.06E-06	3.09E-06	0.95
5	3.99E-06	4.03E-06	0.85
6	5.03E-06	5.07E-06	0.78
7	6.18E-06	6.23E-06	0.72
8	7.47E-06	7.53E-06	0.67
9	8.96E-06	9.02E-06	0.65
10	1.07E-05	1.08E-05	0.43

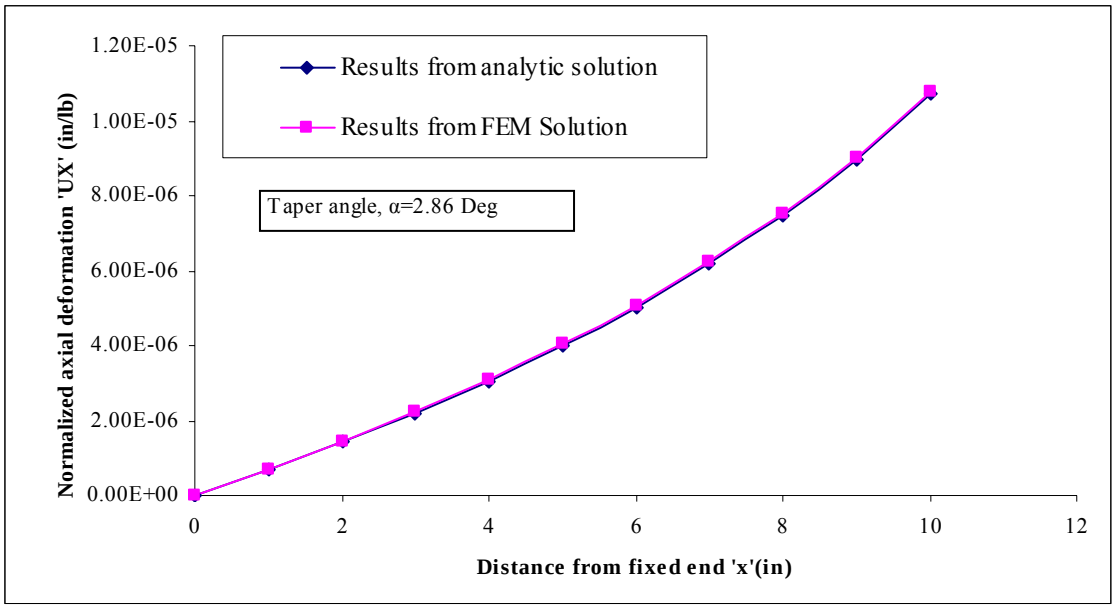

Fig 3.5 Graph of Normalized Displacement Vs Distance from Fixed End

3.4 Analytical Model of the Composite Tube

3.4.1 Geometry

Consider a tapered tube with mid-thickness larger radius R_L, mid-thickness smaller radius R_S, Length L and a tube thickness t. Consider a section of the tapered tube at a distance 'x' from the larger end, having a mid-thickness radius, R_x. Note that $t = 6\,t_{ply}$ as shown in *Fig 3.6*.

3.4.2 Stiffness Matrices

The composite tapered tube as we know does not have a uniform radius, but the radius varies linearly with the distance. Hence the stiffness matrices for the tube given in

equation 3.13 have to be written in terms of R_x, where R_x is the mid-thickness radius of the tube at any section.

$$\left[\bar{A}\right] = R_x \int_0^{2\pi} \left[A'\right]\, d\theta$$

$$\left[\bar{B}\right] = R_x \int_0^{2\pi} \left[B'\right]\, d\theta \qquad (3.9)$$

$$\left[\bar{D}\right] = R_x \int_0^{2\pi} \left[D'\right]\, d\theta$$

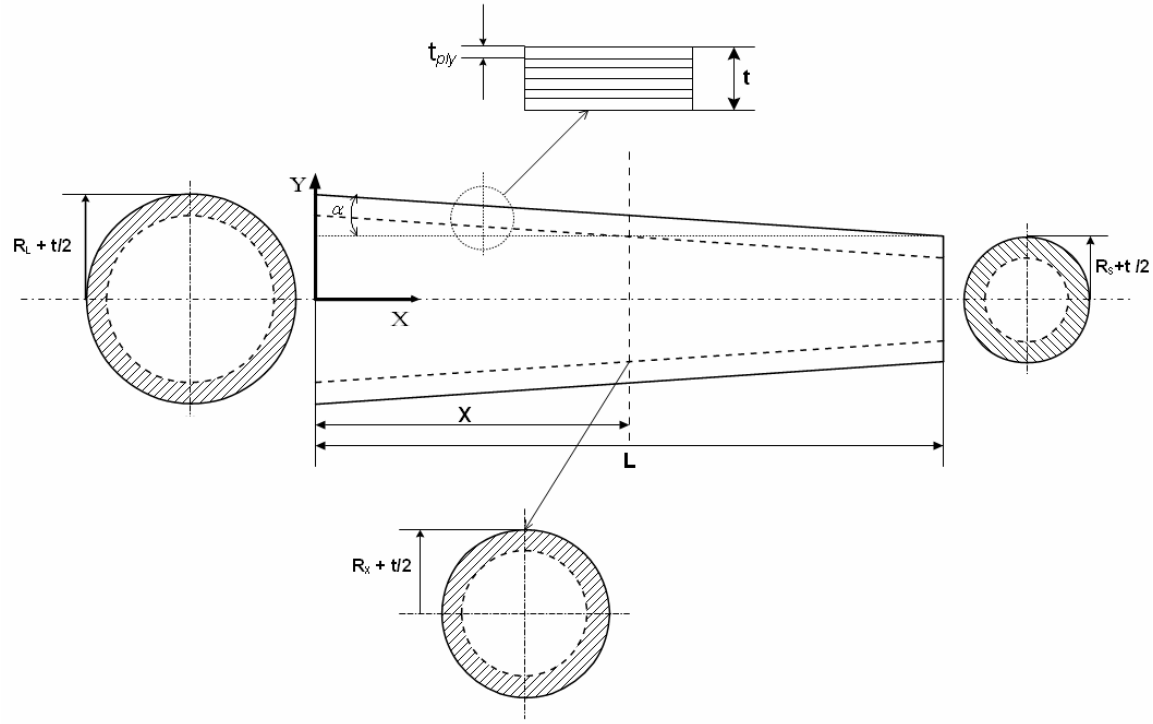

Fig 3.6 Geometry of the Tapered Composite Tube

The individual terms of the $\left[\bar{A}\right], \left[\bar{B}\right]$ and $\left[\bar{D}\right]$ are given in Appendix A.

Note that the reduced stiffness matrices $\overline{Q}_{ij}$ of the plies are not only dependent on the fiber orientation angle β and the elastic constants of the composite material, but are also dependent on the orientation angle θ of the infinitesimal element with the z axis. The orientation angle term, θ, however vanishes during the integration over the θ domain. *Fig 3.7* shows a flow chart of the complete procedure of finding the analytical model for axial and torsion deformation for a tapered laminated composite tube. Note that the order of the transformation has no effect on the final stiffness matrices of the tube.

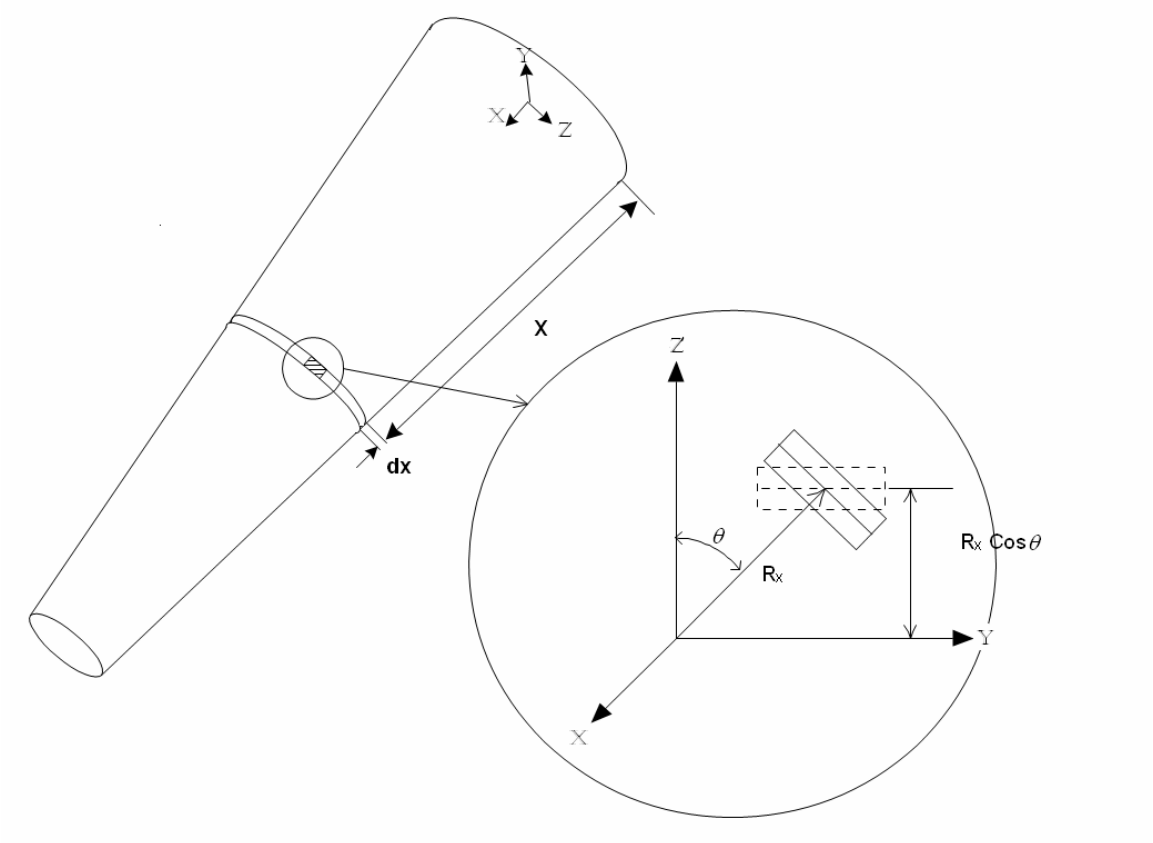

Fig 3.7 Development of the Analytical Model from the Laminated Plate Theory

3.4.3 Axial stiffness and Stress Distribution

From equation 2.8, we saw that the axial deformation for a uniform laminated composite tube is given by

$$\varepsilon_0^x = \bar{a}_{11}\ N_x \tag{3.10}$$

Where, N_x is the total force in the x direction.

For a tapered tube, the axial deformation has to be integrated with respect to x since $\bar{a}_{11}$ is a function of x. The total axial deformation is thus given by:

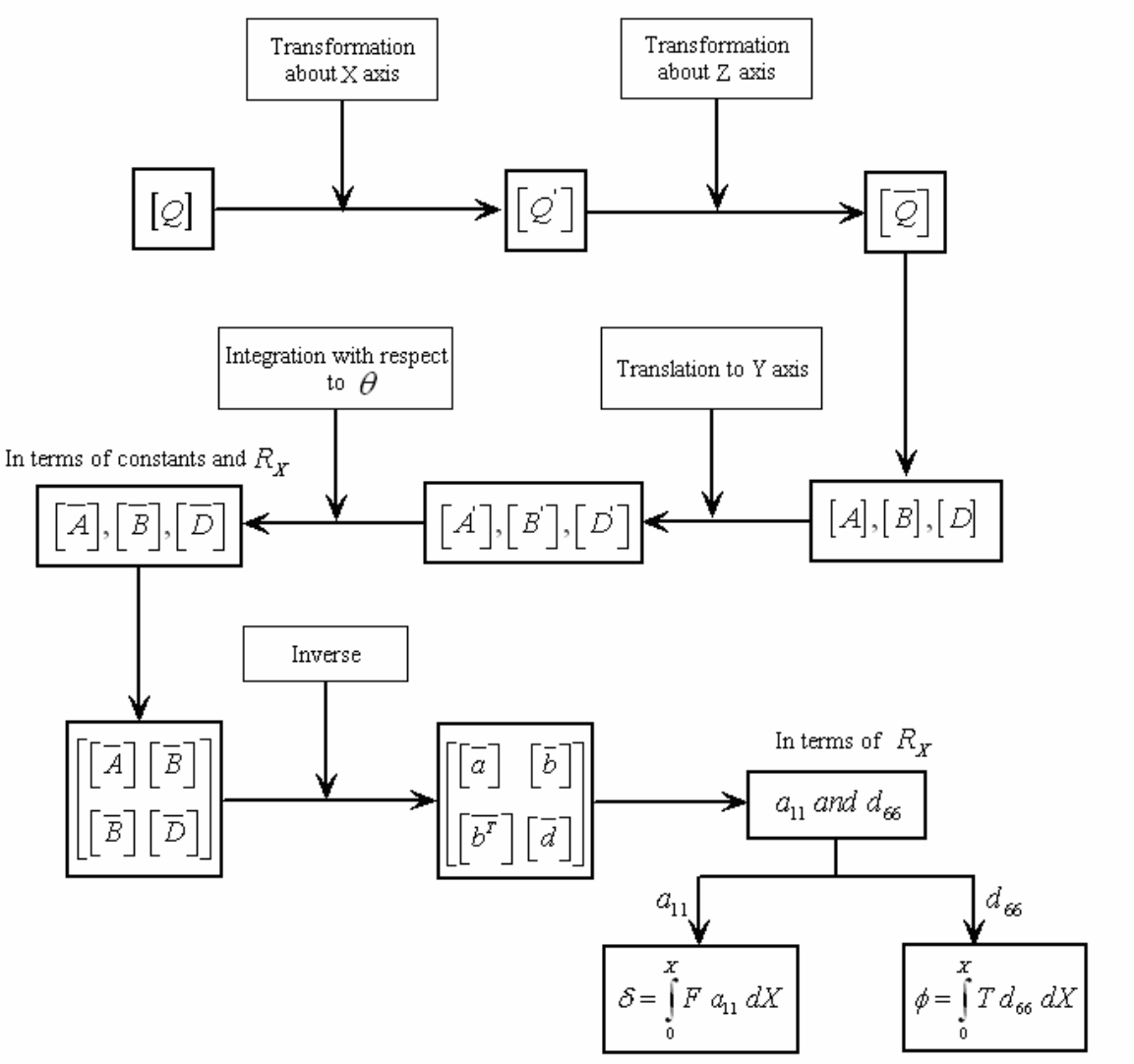

Fig 3.8 Flow Chart of the Development of the Analytical model

$$\delta_x = \int_0^x F\ a_{11}\ dX \tag{3.11}$$

Note that the deformation remains the same at all points in a cross sectional plane.

From the equation for A_{11} as given in Appendix A, we can see that the term A_{11} has a unit lb. Hence a_{11} is of the unit, $\frac{1}{lb}$. The product of force F and a_{11} which is dimensionless is integrated with respect to x. Thus we can see that the equation on the right has a dimension of in.

For a tube of uniform wall thickness, the $\left[\bar{B}\right]$ matrix will be zero, irrespective of whether the lay-up is symmetric or asymmetric implying that there is no extension-bending coupling in a laminated tube. Hence, $\left[\bar{a}\right] = \left[\bar{A}\right]^{-1}$. Since, $\left[\bar{A}\right]$ is a function of the laminate constants and R_x, R_x can be taken out and the laminated constants can be substituted to give $\bar{a}_{11}$ in the form of $\frac{1}{R_x}$ multiplied by constant.

$$\bar{a}_{11} = \frac{1}{R_x} \cdot C$$

The constant C can be found out by substituting the elastic constants in the $\bar{A}$ terms and then obtaining the first row, first column term of the matrix, $\left[\bar{a}\right]$. Thus the axial deformation of the tube can be written as:

$$\delta_x = \frac{FC}{\tan\alpha} \ln\left(\frac{R_L}{\left(R_L - x\tan\alpha\right)} \right) \tag{3.12}$$

Note that the a_{11} term is a function of R_x, which is given by:

$$R_x = R_L - x\tan\alpha$$

The equation 3.11 is analogous to the equation for an isotropic tube given in Section 3.1, where a_{11} is replaced by $\frac{1}{E A_x}$. Note that the a_{11} term takes into account the material properties and the effect of curvature.

3.4.4 Calculation of the Stresses from Analytical Solution

The analytical model developed is further validated for stresses in the layers. The stresses are computed as follows.

We know that,

$$\begin{bmatrix} \varepsilon_0 \\ \kappa \end{bmatrix} = \begin{bmatrix} \bar{a} & \bar{b} \\ \bar{b}^T & \bar{d} \end{bmatrix} \cdot \begin{bmatrix} N \\ M \end{bmatrix} \tag{3.13}$$

.

For a laminate tube with uniform thickness, $\left[\bar{b}\right] = 0$. For the tension case, only N_x will be applied. Hence, $\left[\kappa\right] = 0$ and $\left[\varepsilon_0\right] = \left[\bar{a}\right] \cdot \left[N\right]$. Hence, for any section, stresses in the global co-ordinate system are given by:

$$[\sigma]_{1-2} = \left[\bar{Q}\right]_{x-y} \cdot \left[\bar{a}\right] \cdot [N]$$

The $\left[\bar{a}\right]$ matrix is a function of R_x and can be found out for different sections by changing x from 0 to L.

3.5 Finite Element Model of the Composite Tapered Tube

3.5.1 Geometry of the tube

A tube made of $IM\,6/3501-6$ Graphite Epoxy composite with a lay-up $\left[\pm 45/0\right]_S$ is considered. The dimensions of the tube are same as the isotropic case as described in Section 3.2.1. The ply thickness $t_{ply} = 0.005$ in

The composite material $IM\,6/3501-6$ has the following properties.

$$E_1 = 22.8E6\ psi;\ E_2 = 1.35E6\ psi;\ E_3 = 1.35E6\ psi$$
$$\nu_{12} = 0.3;\ \nu_{23} = 0.34;\ \nu_{13} = 0.3;$$
$$G_{12} = 0.83E6\ psi;\ G_{23} = 0.504E6\ psi;\ G_{13} = 0.83E6\ psi$$

3.5.2 Meshing the model

3.5.2.1 Element Description

The element used for meshing is SOLID 191, which is the layered version of SOLID95 element. The element has 20 nodes, with UX, UY and UZ degrees of freedom

at each node. The element allows up to 100 layers. If more layers have to be input, elements have to be stacked. *Fig 3.9* shows the geometry of the Solid 191 Element.

The material properties can be input in two ways. The first method is to input the material constants and defining the lay-up of the laminate. The second method is to input the laminate constitutive matrix, which is computed by an external program.

While creating the model, care has to be taken in order to insure that the *z* co-ordinate is oriented along the thickness.

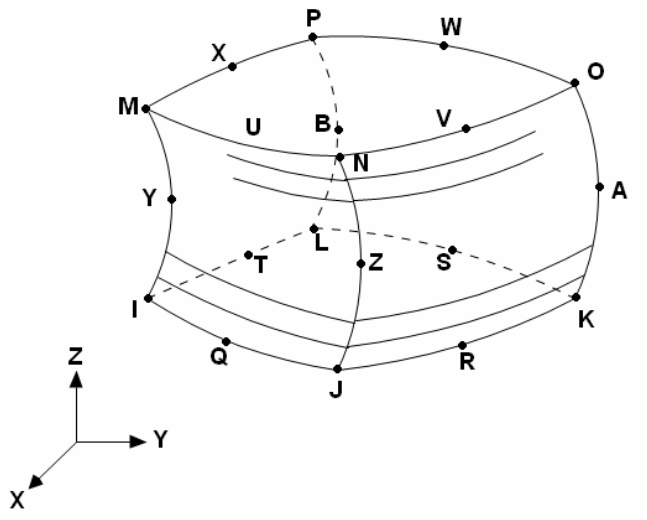

Fig 3.9 Solid 191 Element Geometry

3.5.2.2 Generation of the Model

6 volumes, corresponding to 6 plies are created in the model. A real constant set is defined for each ply and assigned to the corresponding volume using the *VATT* command. The volumes are naturally glued to each other because of the method of

creation of volumes. The mesh sizes, obtained from the convergence test are specified in order to ensure that correct results are obtained from finite element method.

3.5.3 Boundary Conditions

The model is constrained at the larger (left) end for UX only. A rigid region is created at the smaller end using the CERIG command. A force *FX* of 500 lb is applied on the master node.

3.6 Results Comparison

Since a rigid region is created, all nodes in a section have the same displacement. The values of UX, which is the deformation in *x* direction at 11 different sections are tabulated and compared with the analytical solution. *Table 3.3* gives the comparison between the analytic solution results and the finite element results. *Fig 3.10* shows the graph of normalized axial deformation versus distance from fixed end

Fig 3.11 shows the axial deformation of the tapered tube at its tip. It is shown that unlike a uniform tube, non linear deformation along the length direction is obtained.

Table 3.3 Comparison of normalized axial deformation from analytical method and finite element method for a composite tube

Distance from Fixed End (in)	Normalized UX- FEM (in/lb)	Normalized UX- Analytic (in/lb)	% Difference
1	7.94E-07	8.14E-07	2.52
2	1.60E-06	1.71E-06	6.88
3	2.47E-06	2.65E-06	7.29
4	3.41E-06	3.68E-06	7.80
5	4.45E-06	4.80E-06	7.98
6	5.58E-06	6.06E-06	8.57
7	6.85E-06	7.44E-06	8.65
8	8.28E-06	9.00E-06	8.75
9	9.92E-06	1.08E-05	8.91
10	1.18E-05	1.29E-05	9.05

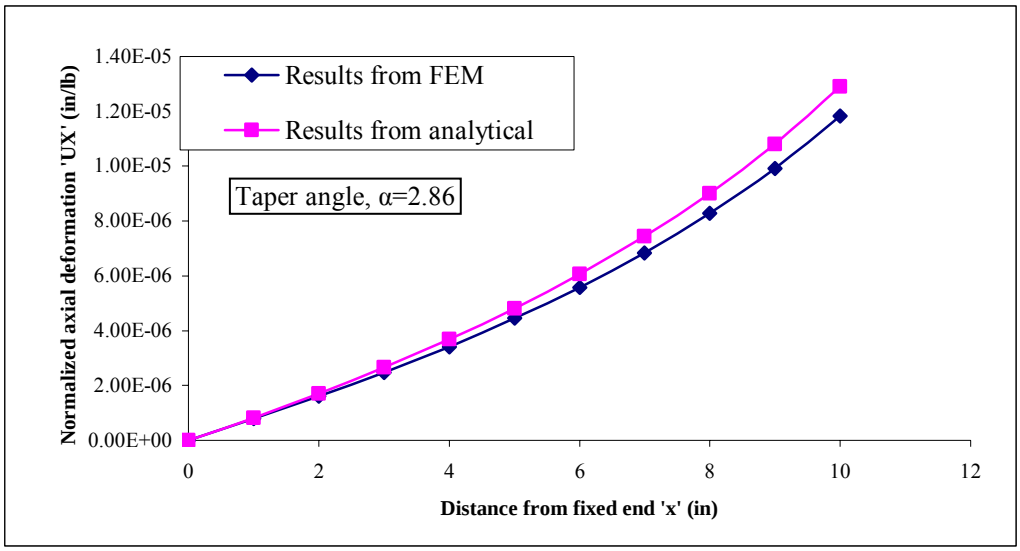

Fig 3.10 Graph of axial deformation vs. distance from fixed end for the composite tube

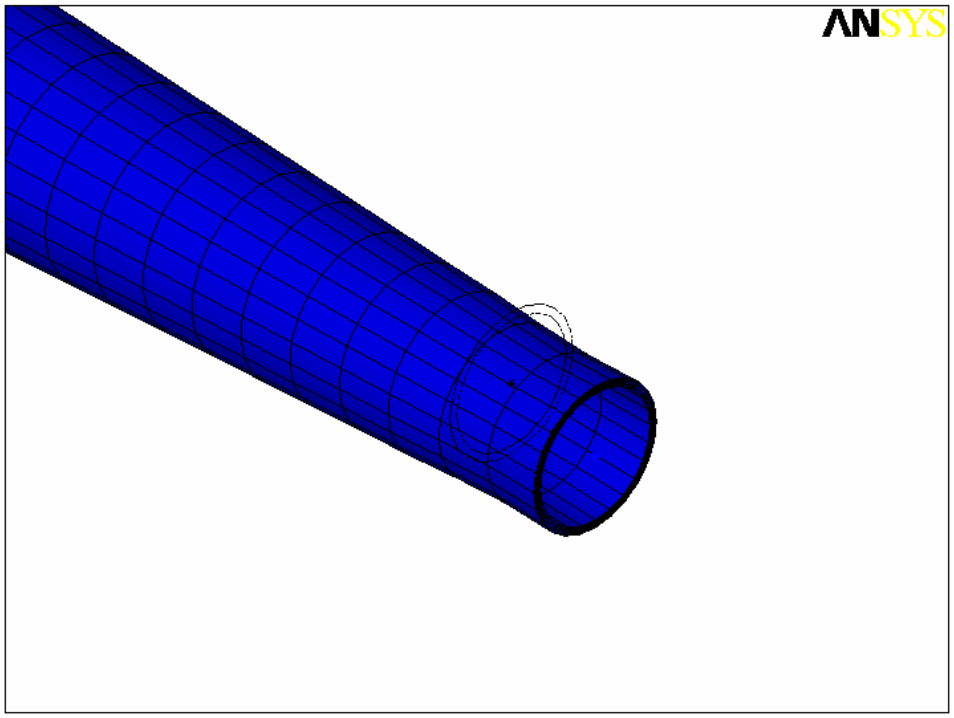

Fig 3.11 Plot showing the displacement of the tip of the tapered tube

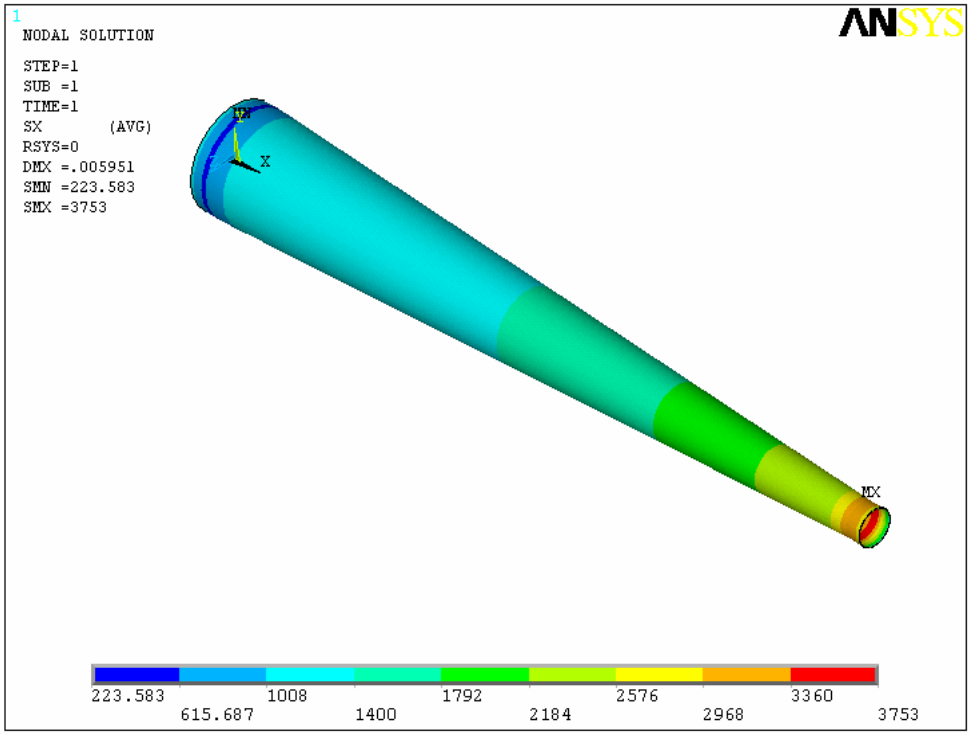

Fig 3.12 Stresses along the x direction in the $+45^0$ ply

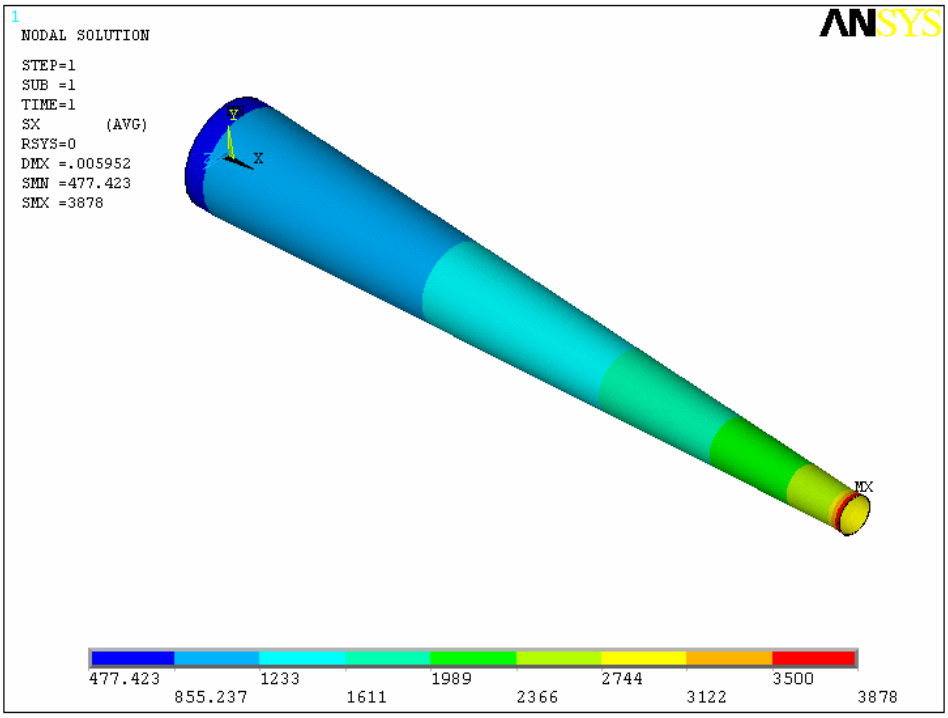

Fig 3.13 Stresses along the x direction in the -45^0 ply

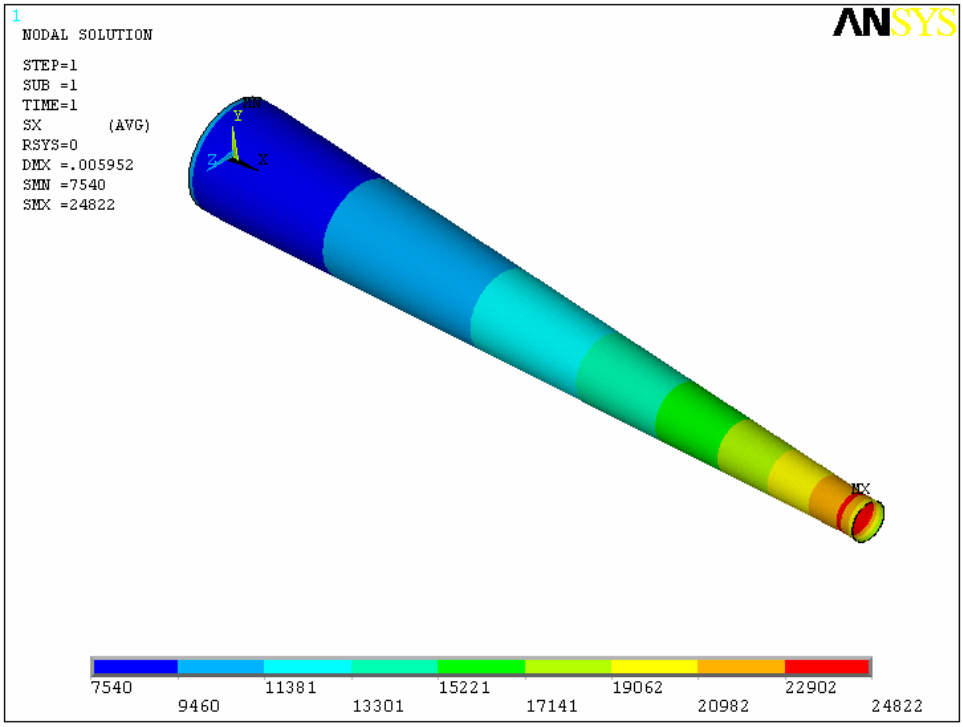

Fig 3.14 Stresses along the x direction in the 0^0 ply

Figs. 3.12, 3.13 and *3.14* show the stresses along the x direction in $+45^0$, -45^0 and 0^0 plies starting from the innermost layer. It can be seen that the maximum stresses occur at the smallest cross section. This is however not the tip of the tube, since after deformation, the area of the tip of the tube is enlarged. It can be observed that the maximum stresses of the $+45^0$ and the -45^0 plies are close; Comparing figures *3.12, 3.13* and *3.14* we can find that the 0^0 layer has the highest maximum stresses.

3.6.1 Comparison of Axial Stresses

Stresses are calculated in the $+45^0$ layer using the analytical model developed in *Section 3.5.1* and are compared with the finite element results. The results are tabulated in *Table 3.4*

Table 3.4 Comparison of stresses

Stresses	Analytical solution (psi)	Finite element method (psi)
x=5	1463	1468.5
x=10	3155.3	3187.9

CHAPTER 4

TAPERED TUBES UNDER TORSION

4.1 Analytical Solution for an Isotropic Tube

Consider a tapered tube with geometry as mentioned in Section 3.1. The radius of the tube at a distance x from the fixed end R_x is given by:

$$R_x = R_L - x\tan\alpha\,,$$

Where α the taper is angle of the tube and $\tan\alpha = \frac{\Delta R}{L}$; ΔR is the difference between the radii of the tube;

$$\Delta R = R_L - R_S$$

The polar moment of inertia J_L at the large section of the tube will be given by:

$$J_L = \frac{\pi}{2}\left[\left(R_L + \frac{t}{2}\right)^4 - \left(R_L - \frac{t}{2}\right)^4\right] \tag{4.1}$$

It can be simplified to form

$$J_L = \frac{\pi}{2}\left[4\,R_L^3\,t + R_L\,t^3\right] \tag{4.2}$$

Similarly the polar moment of inertia of the tube at a section x from the fixed end is given by

$$J_x = \frac{\pi}{2}\left[4\ R_x^3\ t + R_x\ t^3\right] \tag{4.3}$$

The angle of twist of a bar with varying cross section at a section, distance x from the fixed end is given by:

$$\phi_x = \frac{T}{G}\int_0^x \frac{dX}{J_x} \tag{4.4}$$

After integration, the angle of twist of the bar at any section is given by:

$$\phi_x = \frac{T}{\pi\, G\ t^3\ \tan\alpha}\cdot \ln\left(\frac{R_L^2\left(t^2 + 4\left(R_L - x\tan\alpha\right)^2\right)}{\left(t^2 + 4R_L^2\right)\left(R_L - x\tan\alpha\right)^2}\right) \tag{4.5}$$

For the limiting case of a cylinder, $\tan\alpha = 0$. Hence using L'Hospitale's rule, we can find the twisting angle as:

$$\phi = \frac{Tx}{G\cdot\frac{\pi}{2}\left(4R^3t + Rt^3\right)}$$

This can be verified from a solid mechanics text book.

A MATHEMATICA program (Appendix C) is used to calculate the angle of twist of a tapered tube with the following dimensions: R_L = 0.765 in; R_S = 0.265 in; L = 10 in; t = 0.03 in;

The results are compared with finite element results and tabulated in *Table 4.1*.

4.2 Finite Element Model of an Isotropic Tube

A tapered tube of dimensions, $R_L = 0.765$ in ; $R_S = 0.265$ in, $L = 10$ in and $t = 0.03$ in is modeled in the same fashion as described in Section 3.2. Appendix (E) shows the ANSYS batch file used for the generation of the model. *Fig 4.1* shows the finite element model of the tapered tube along with the boundary conditions and loads.

4.2.1 Meshing the Model

The same model as described in Section 3.7 is adopted. The model is fixed at the large end for all degree of freedom as shown in *Fig 4.1*. At the smaller end, a rigid region is created using CERIG command. A torque (MX) of 280 lb-in is applied at the master node.

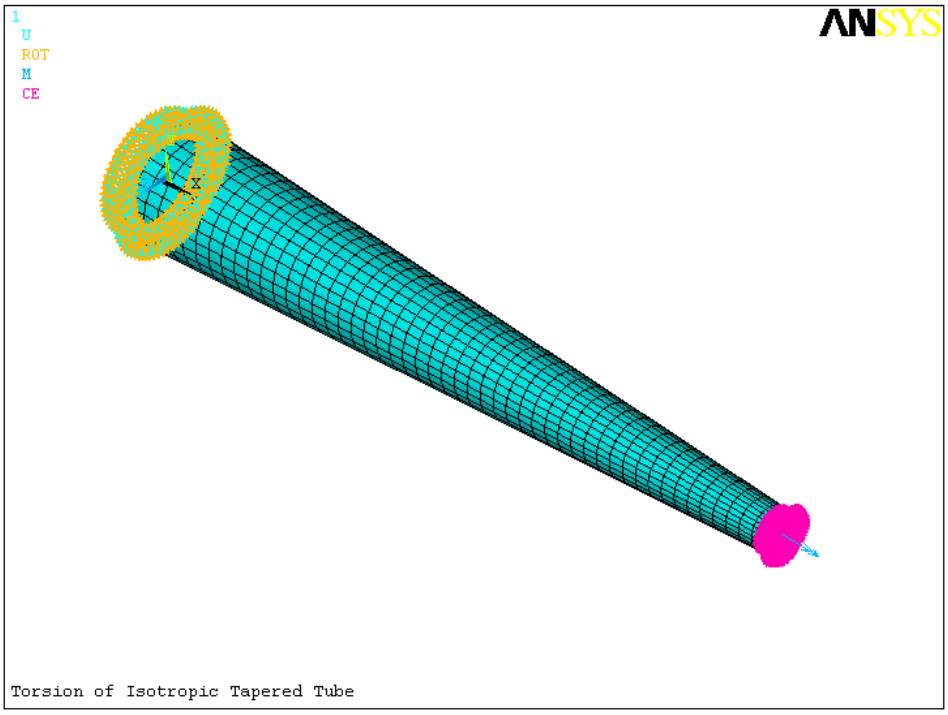

Fig 4.1 Finite Element Model of a Tapered Isotropic Tube under Torsion with Boundary Conditions

4.3 Results Comparison

Table 4.1 shows the comparison of the results obtained from FEM and Analytical solution. *Fig 4.2* shows a graph of normalized angle of twist results versus distance from the fixed end. It can be observed that the finite element model results are very close to the analytical results with a low percentage error of 0.6.

Table 4.1 Comparison of angle of twist results from analytical method and finite element method for an isotropic tube

Distance from the fixed End $x(in)$	Normalized angle of twist- FEM (in/lb)	Normalized angle of twist -Analytic (in/lb)	% Difference
1	3.32E-06	3.32E-06	0.00
2	7.43E-06	7.42E-06	0.13
3	1.25E-05	1.25E-05	0.00
4	1.91E-05	1.91E-05	0.00
5	2.77E-05	2.76E-05	0.36
6	3.92E-05	3.91E-05	0.26
7	5.51E-05	5.50E-05	0.18
8	7.80E-05	7.78E-05	0.26
9	1.13E-04	1.12E-04	0.89
10	1.69E-04	1.68E-04	0.60

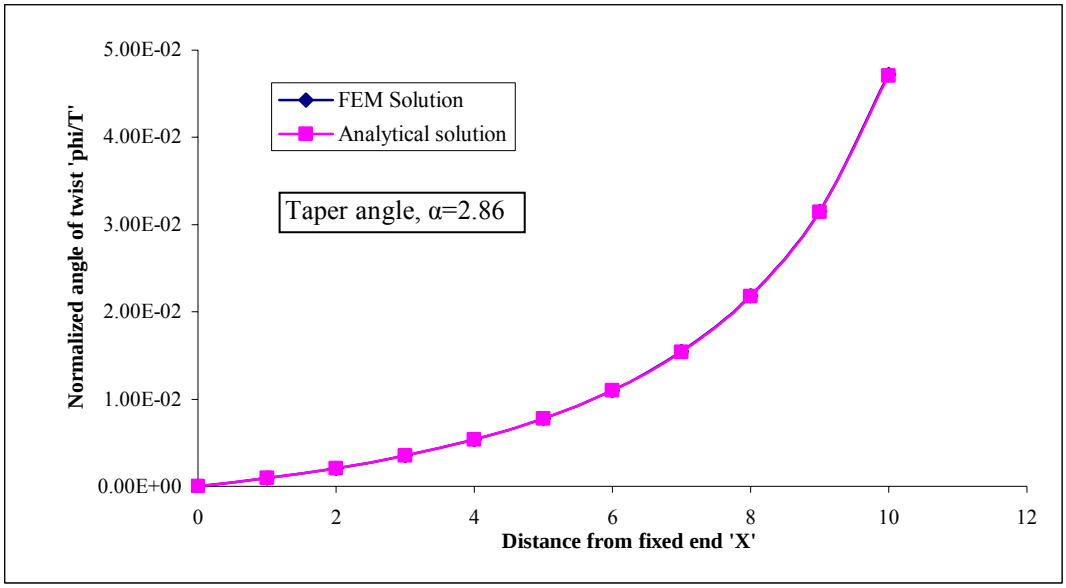

Fig 4.2 Graph showing the normalized angle of twist from analytical and finite element method Vs distance from fixed end

4.4 Analytical Model of the Composite Tube

In Section 3.3, we derived the laminate stiffness equations of the tube $[\bar{A}], [\bar{B}]$ and $[\bar{D}]$ at any section of radius R_x (2.7). We know that the mid-plane strains and curvatures of a laminate are given by:

$$\begin{Bmatrix} \varepsilon_0 \\ k \end{Bmatrix} = \begin{bmatrix} \bar{a} & \bar{b} \\ \bar{b}^T & \bar{d} \end{bmatrix} \begin{Bmatrix} N \\ M \end{Bmatrix} \tag{4.6}$$

where,

$$\begin{bmatrix} \bar{a} & \bar{b} \\ \bar{b}^T & \bar{d} \end{bmatrix} = \begin{bmatrix} \bar{A} & \bar{B} \\ \bar{B} & \bar{D} \end{bmatrix}^{-1}$$

Now, expanding the above matrix for κ_{xy}, we have

$$k_{xy} = \bar{b}_{16}N_x + \bar{b}_{26}N_y + \bar{b}_{66}N_{xy} + \bar{d}_{61}M_x + \bar{d}_{62}M_y + \bar{d}_{66}M_{xy} \tag{4.7}$$

Since in the problem, we are applying only a torque T (M_{xy} in composite terminology), all the terms except $\bar{d}_{66}M_{xy}$ are reduced to zero. Hence,

$$\kappa_{xy} = \bar{d}_{66}M_{xy} \tag{4.8}$$

For the tapered tube, the above equation has to be integrated with respect to x, since the area of the tube varies linearly with respect to x. Hence, the angle of twist at any section, ϕ_x (κ_{xy} in composite terminology) is given by:

$$\phi_x = \int_0^x T\,\bar{d}_{66}\,dx \tag{4.9}$$

Where $T = M_{xy}$ and $\phi_x = \kappa_{xy}$.

Since $\left[\bar{B}\right] = 0$ for a tube of uniform thickness,

$$\left[\bar{d}\right] = \left[\bar{D}\right]^{-1}$$

All the constants are plugged into the $\bar{D}$ matrix terms and then an inverse of the matrix is computed. The $\bar{d}_{66}$ term is then a function of R_x^3 and R_x. This is further used in the integration to compute the angle of twist at any section. Note that in case of a laminate, M_{xy} has a unit of $lb - \frac{in}{in}$, but in case of the tapered tube, T or M_{xy} has units $lb - in$. Note that term $\bar{d}_{66}$ has a unit of, $\frac{1}{lb - in^2}$. Thus the angle of twist has a unit of rad.

4.4.1 Stress Calculations

For a tube of uniform laminate, $\left[\overline{B}\right] = 0$. Hence, from equation 3.13, $\left[\kappa\right] = \left[\overline{d}\right] \cdot \left[M\right]$. In the torsion case only M_{xy} is present. Hence, the stresses, can be found as:

$$\left[\sigma\right]_{x-y}^{k} = \left[\overline{Q}\right]_{k} \cdot z_k \cdot \left[\overline{d}\right] \cdot \left[M\right] \tag{4.10}$$

Using this method, stresses are calculated for the plies. Note that in the above equation, z_k is the distance of the surface from the mid-section of the tube.

4.5 Finite Element Model of the Composite tube

The tapered tube model generated in Section 3.7 is used in the torsion case as well. The boundary conditions applied are however different in this case. The tube is fixed for all DOF at the larger end as shown in *Fig 4.1*. At the smaller end, a rigid region is created using *CERIG* command. A torque $T = 280\ lb - in$ is applied on the master node. The model is then solved for its stresses and strains.

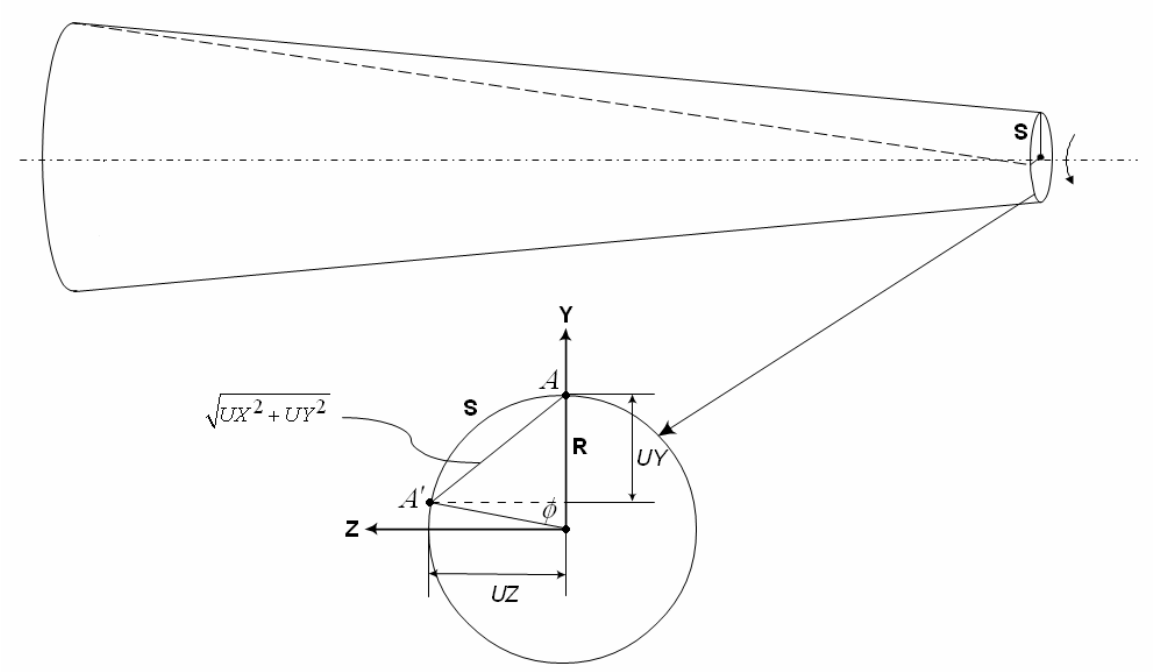

Fig 4.3 Calculation of the Angle of twist from Finite Element Model

4.5.1 Post Processing and Results Comparison

The angle of twist ϕ can be obtained from the post processor as nodal solution for *ROTX* . However, these results are not calculated at every node. Hence a manual method for calculation of ϕ is adopted.

Refer to *Fig 4.3*. Under the application of a torque, the point on the circumference moves from A to A'. The angle swept is the angle of twist ϕ and S is the arc length. Now, we know that the arc length is given by, $S = R\,\phi$, where R is the radius. The arc length S will be approximately equal to the hypotenuse AA'. Hence, $S \sim \sqrt{UY^2 + UZ^2}$. Thus angle of twist, $\phi \sim \dfrac{\sqrt{UY^2 + UZ^2}}{R}$. UY and UZ are the displacements in Y and Z respectively, obtained from the post processor.

Table 4.2 shows the results comparison between analytic solution and Finite Element Method for the angle of twist of a laminated tapered tube. *Fig 4.4* shows the comparison of the angle of twist solution between analytical and finite element methods for different sections of the tube.

Table 4.2 Comparison of angle of twist results from analytical method and finite element method for a composite tube

Distance from fixed End $x(in)$	Normalized ϕ from FEM ($rad/lb-in$)	Normalized ϕ from Analytic ($rad/lb-in$)	% Difference
1	3.771E-06	3.929E-06	4.16
2	8.312E-06	8.679E-06	4.41
3	1.404E-05	1.471E-05	4.78
4	2.137E-05	2.250E-05	5.29
5	3.092E-05	3.286E-05	6.23
6	4.372E-05	4.714E-05	7.83
7	6.140E-05	6.679E-05	8.76
8	8.680E-5	9.482E-05	9.24
9	1.252E-04	1.386E-04	9.28
10	1.865E-04	2.089E-04	11.63

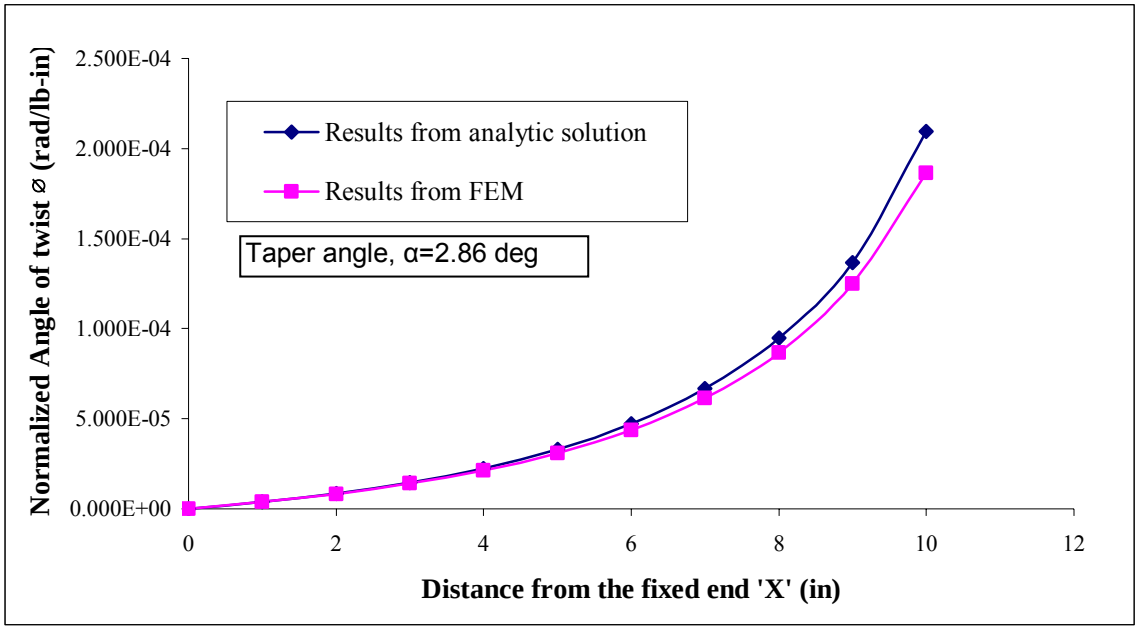

Fig 4.4 Graph of normalized angle of twist vs. Distance from fixed End

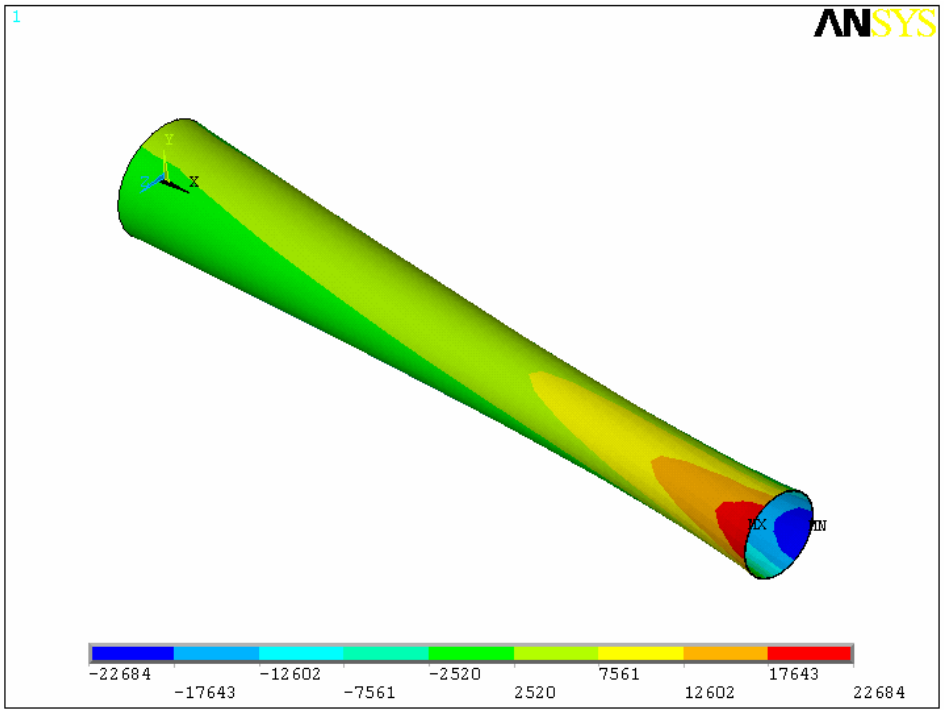

Fig 4.5 Shear stresses on the $+45^0$ ply

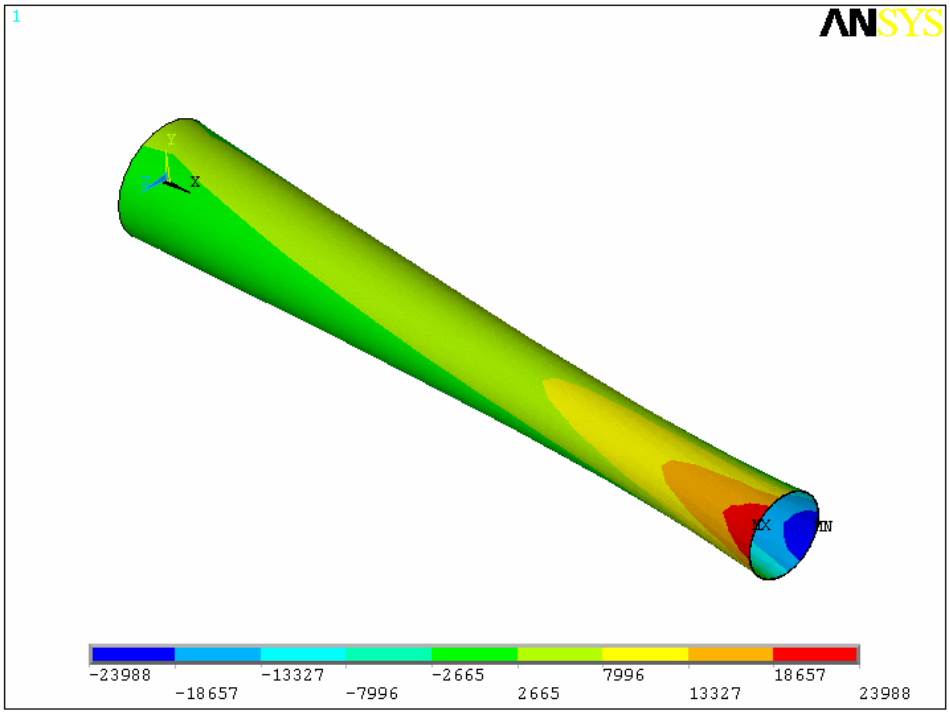

Fig 4.6 Shear stresses on the -45^0 ply

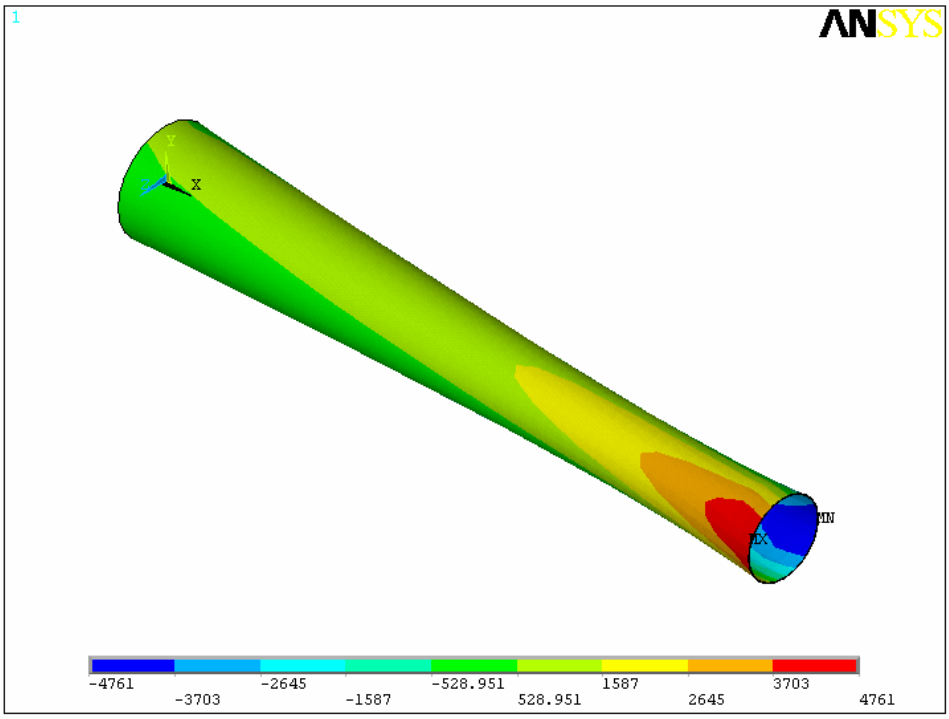

Fig 4.7 Shear stresses on the 0^0 ply

Fig.s 4.5, 4.6 and 4.7 show the shear stress plots of the $+45^0$, -45^0 and 0^0 plies. It can be seen that the $+45^0$ and the -45^0 plies have nearly the same maximum stresses. Also, the 0^0 layer has lesser maximum stress than the $+45^0$ and the -45^0 layers. This can be explained because the 0^0 layer has lesser equivalent shear modulus; hence higher shear deformation and hence lesser stresses.

4.5.2 Comparison of Shear Stresses (τ_{xy})

Stresses from the analytical method are found using 4.10. Stresses are evaluated for the $+45^0$ (innermost) layer at two different sections. *Table 4.3* shows the comparison of shear stresses between the analytical and FEM results.

Table 4.3 Comparison of Shear stresses

Stresses	Analytical solution (psi)	Finite element method (psi)
$x=5$	5998	6041
$x=10$	22576	22684

It can be seen from the table that the results are in good agreement with each other.

CHAPTER 5

PARAMETRIC STUDIES

The geometry of the tube, stacking sequence, taper angle, fiber orientation etc. play an important role in the stiffness of composite tubes. In this study, an effort has to be done to study the effects of these on the deformations of the tube. IM6/3501-6 Graphite Epoxy composite is used for these studies. A tube with dimensions as described in *Section 3.6.1* is considered for the analysis.

5.1 Stacking Sequence Effect

5.1.1 Axial Case

In this section, the effect of stacking sequence on the axial deformation of the tube is studied. To examine the effects, three laminates having the same fiber orientations, but different arrangement is considered. $[\pm 45/0]_S$, $[0/\pm 45]_S$ and $[+45/0/-45]$ are the three lay-ups considered. The variation of the analytical solution for the three lay-ups is seen. MATHEMATICA program (Appendix D) is used for the calculation of the results, which are tabulated in *Table 5.1*

Table 5.1 Variation of axial deformation with stacking sequence

Lay-Up	Normalized Axial Deformation 'δ / F' (in/lb)
$[\pm 45/0]_S$	1.294E-4
$[0/\pm 45]_S$	1.294E-4
$[+45/0/-45]$	1.294E-4

It can be seen that the stacking sequence has no effect on the axial deformation of the tapered tube. This can be explained, because the extensional stiffness matrix of the tube $[\bar{A}]$ does not vary with the arrangement of the plies.

5.1.2 Torsion Case

Here, the effects of stacking sequence on the torsion deformation (twisting angle) are studied. The same lay-ups as in *Section 5.1.1* are considered. The results are generated using the MATHEMATICA code (Appendix D). *Table 5.2* shows the angle of twist results for the different lay-ups.

Table 5.2 Variation of angle of twist with stacking sequence

Lay-Up	Normalized Angle of twist ϕ / T (rad/lb-in)
$[\pm 45/0]_S$	3.2646E-04
$[0/\pm 45]_S$	3.2676E-04
$[+45/0/-45]$	3.2675E-04

It can be observed from the table that stacking sequence has little effect on the angle of twist of the tapered tube. The twisting angle is dependent on the torsional stiffness of the tube cross section. The torsional stiffness of the laminate $\frac{1}{d_{66}}$ does not depend on the stacking sequence. However, the torsional stiffness of the tube is predominant by the $\left[\overline{A}\right]$ matrix, which is independent of stacking sequence. As a result, the twisting angle has little effect on the stacking sequence of the laminate.

5.2 Effect of Fiber Orientation

5.2.1 Axial case

One of the important properties of laminated composite materials is their directional dependence, which facilitates a design which can be tailored to the application. This property is exploited in almost all the applications of laminated composites. In the current study, symmetric lay-ups with $+\theta^{\circ}, -\theta^{\circ}$ and 0° plies are considered. θ values are changed from 15° to 75° with an increment of 15°. The MATHEMATICA code (Appendix D) is used to calculate the results. Results are tabulated in *Table 5.3*

Table 5.3 Variation of axial deformation with fiber orientation

Lay-Up	Normalized Axial Deformation δ / F (in/lb)
$[\pm 15/0]_s$	5.888E-6
$[\pm 30/0]_s$	9.982E-6
$[\pm 45/0]_s$	1.295E-5
$[\pm 60/0]_s$	1.383E-5
$[\pm 75/0]_s$	1.405E-5

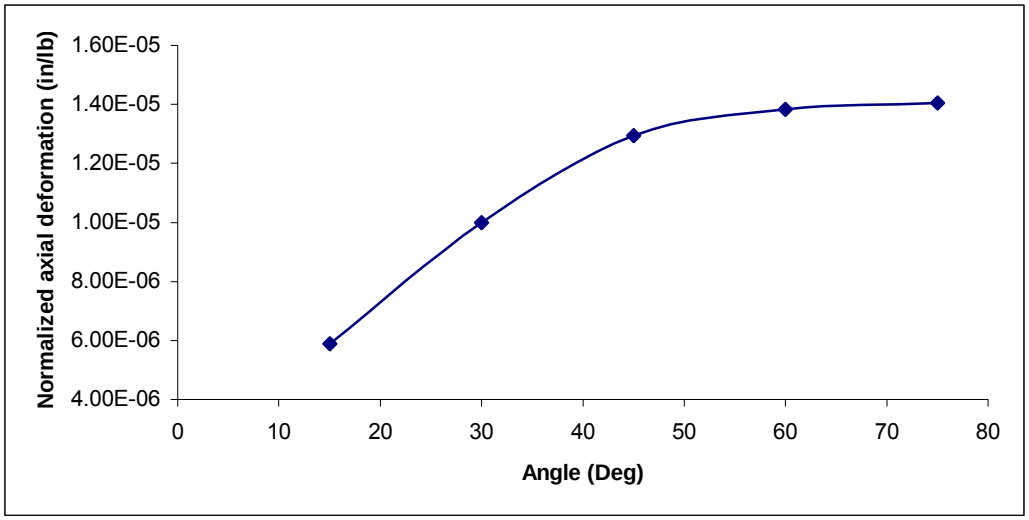

Fig 5.1 Variation of axial deformation with fiber orientation

It can be observed from the table that the deformation is smallest for the 15° orientation and increases with the fiber orientation. This can be accounted for by the fact that a 15° orientation is stiffer in the x direction, since fiber direction and loading directions are separated by a small angle. As the fiber orientation increases the fiber direction becomes almost transverse to the loading direction and hence the stiffness in loading direction (x) becomes less.

5.2.2 Torsion Case

The effects of fiber orientation are studied in this section. The same fiber orientations as in Section 5.2.1 are considered. Normalized angle of twist are computed using the MATHEMATICA code (Appendix D) for the different orientations. The results are tabulated in *Table 5.4*

Table 5.4 Variation of angle of twist with fiber orientation

Lay-Up	Normalized angle of twist ϕ / T (rad/lb)
$[\pm 15/0]_S$	1.017E-4
$[\pm 30/0]_S$	4.709E-5
$[\pm 45/0]_S$	3.712E-5
$[\pm 60/0]_S$	4.709E-5
$[\pm 75/0]_S$	1.017E-4

From *Fig 5.2*, we can observe that the angle of twist is the least for the 45° orientation. Also, the angle of twist is the same for complementary angle orientations ($\theta_1 + \theta_2 = 90^\circ$); For eg., 30° and 60° orientations have the same angle of twist.

This can be explained by the fact that the equivalent shear modulus G_{xy} is the least for 45° orientation as shown in *Fig. 5.3.*

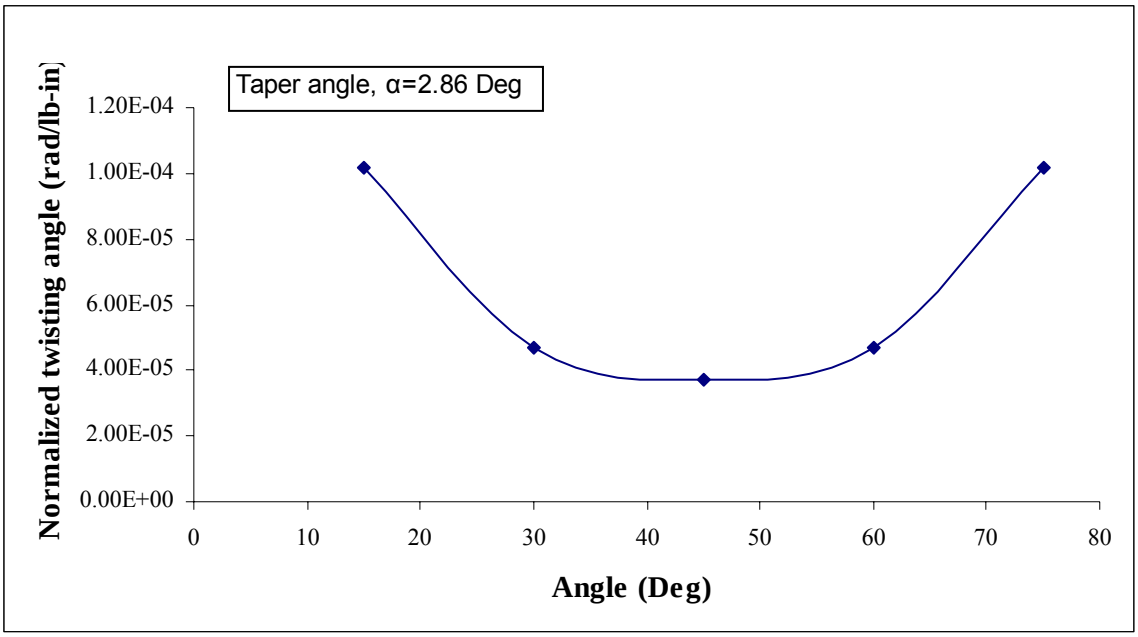

Fig 5.2 Variation of angle of twist with fiber orientation

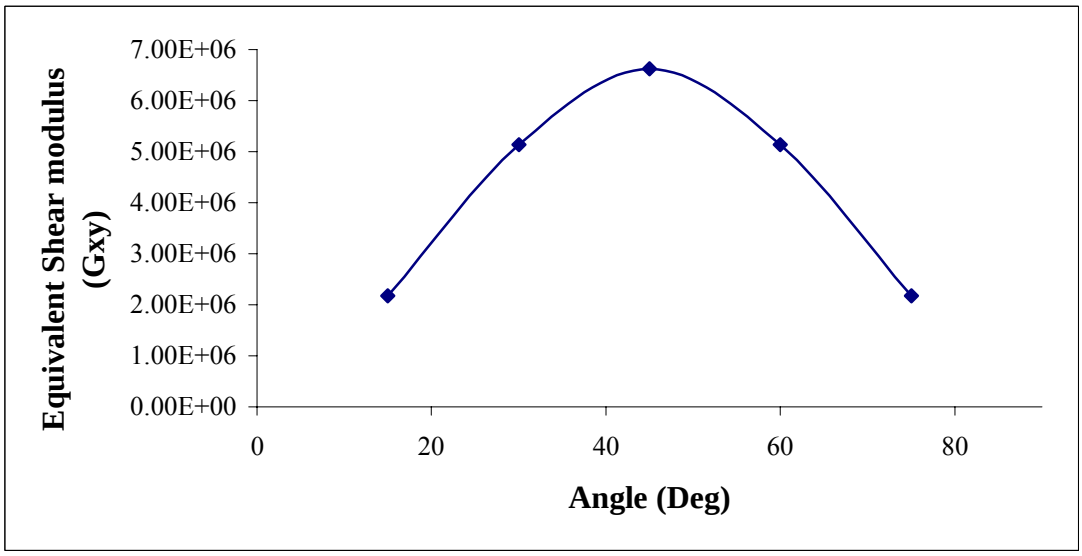

Fig. 5.3 Equivalent shear modulus plot

5.3 Effect of the Taper Angle

5.3.1 Axial case

In this section, the effects of taper angle, α on the deformations of the tube are studied. For a large taper angle, the fiber orientation in the ply does not remain uniform, which results in erroneous results. The MATHEMATICA code given in Appendix D is used for the calculation; the results are tabulated in *Table 5.5*. For the calculation, the larger radius R_L is kept constant and the smaller radius R_S varied accordingly.

Table 5.5 Variation of axial deformation with taper angle α

Taper angle rad (Deg)	Normalized Axial Deformation (in/lb)
0.099 (5.67)	9.713E-06
0.162 (9.28)	1.107E-05
0.219 (12.55)	1.219E-05
0.275 (15.76)	1.315E-05
0.328 (18.79)	1.402E-05
0.381 (21.83)	1.476E-05
0.433 (24.81)	1.544E-05
0.485 (27.79)	1.606E-05

Fig 5.4 shows the graph of variation of deformation with radius ratio. It can be seen that for tubes with low taper angles, the deformation of the bar is less. This is because tubes with low taper angles are nearly cylindrical in nature and are stiffer than tubes with high taper angle.

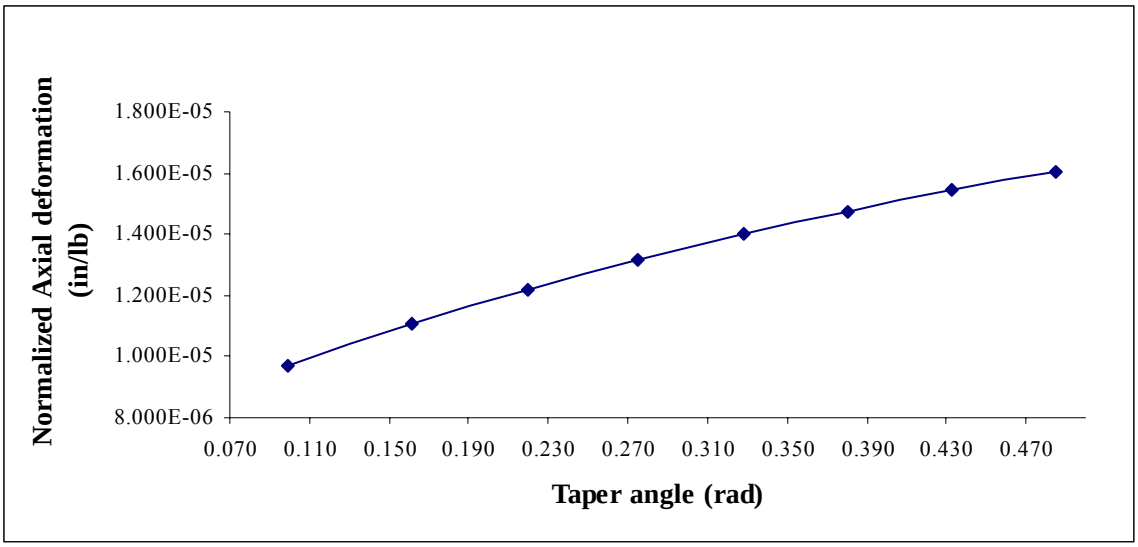

Fig 5.4 Variation of normalized axial deformation with taper angle

5.3.2 Torsion case

The variation of angle of twist for tapered tubes with different taper angles α is studied here. For the calculations, the larger radius R_L is kept constant and the smaller radius R_S varied accordingly. Taper angles varying from 0.099 to 0.485 are used to compute the normalized angle of twist. The results are tabulated in *Table 5.6.*

From the *Fig 5.5*, we can observe that the twisting angle increases with the increase in the ratio. Low taper angle tubes are stiffer than high taper angle tubes and hence have lesser deformation.

Table 5.6 Variation of angle of twist with taper angle α

Taper angle *rad* (*Deg*)	Normalized Angle of twist ϕ / T (rad/lb)
0.099 (5.67)	1.092E-04
0.162 (9.28)	1.748E-04
0.219 (12.55)	2.548E-04
0.275 (15.76)	3.494E-04
0.328 (18.79)	4.607E-04
0.381 (21.83)	5.822E-04
0.433 (24.81)	7.204E-04
0.485 (27.79)	8.730E-04

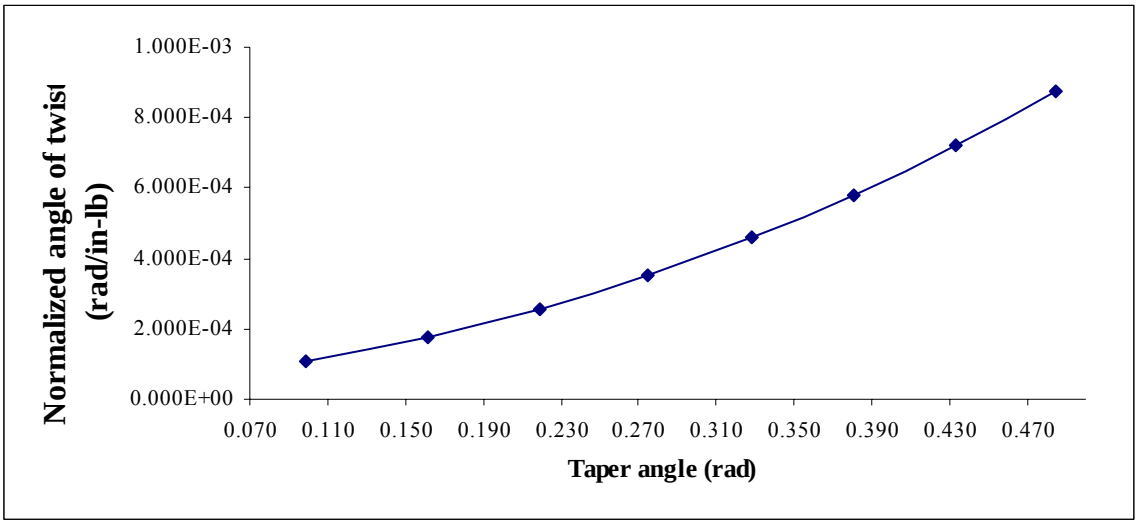

Fig 5.5 Variation of normalized angle of twist with taper angle

CHAPTER 6

CONCLUSIONS

An analytical model for the deformation of tapered laminated composite tubes under axial tension and torsion was developed in this research. The derivation was based on the Laminated Plate approach. The results from analytical model are compared with the results from finite element method. From this research, the following conclusions can be made.

- The axial deformation and the twisting angle for composite tube under axial load and twisting moment respectively predicted by the current developed method agree well with the results obtained from finite element analysis.
- The axial stresses and the shear stress for each ply are also in excellent agreement with the results obtained from the finite element method.
- Angle of twist can be minimized by incorporating 45^{o} plies.
- Axial deformation of composite tubes can be minimized by incorporating near 0^{o} plies.
- Given the set of plies, they can be stacked in any order since the sequence does not affect the deformations significantly.
- Tubes with less taper angle can be employed to minimize the deformations in structural applications.

APPENDIX A

TERMS OF THE STIFFNESS MATRICES

Note : $c_z = \cos\theta; s_z = \sin\theta;$ *Transformation terms w.r.to z*

$$\bar{A}_{11} = 2\pi R_X \sum_{k=1}^{n}\left[c_z^4 Q_{11} + s_z^2 c_z^2\left(Q_{12}+2Q_{66}\right)+\frac{3}{8}s_z^4 Q_{22}\right]_k \cdot\left(z_k - z_{k-1}\right)$$

$$\bar{A}_{12} = 2\pi R_X \sum_{k=1}^{n}\left[s_z^2 c_z^2\left(Q_{11}+\frac{3}{8}Q_{22}-2Q_{66}\right)+\frac{1}{2}\left(s_z^4+c_z^4\right)Q_{12}\right]_k \cdot\left(z_k - z_{k-1}\right)$$

$$\bar{A}_{22} = 2\pi R_X \sum_{k=1}^{n}\left[s_z^4 Q_{11} + s_z^2 c_z^2\left(Q_{12}+2Q_{66}\right)+\frac{3}{8}c_z^4 Q_{22}\right]_k \cdot\left(z_k - z_{k-1}\right)$$

$$\bar{A}_{16} = 2\pi R_X \sum_{k=1}^{n}\left[s_z c_z^3\left(Q_{11}-\frac{1}{2}Q_{12}-Q_{66}\right)+s_z^3 c_z\left(\frac{1}{2}Q_{12}-\frac{3}{8}Q_{22}+Q_{66}\right)\right]_k \cdot\left(z_k - z_{k-1}\right)$$

$$\bar{A}_{26} = 2\pi R_X \sum_{k=1}^{n}\left[c_z s_z^3\left(Q_{11}-\frac{1}{2}Q_{12}-Q_{66}\right)+c_z^3 s_z\left(\frac{1}{2}Q_{12}-\frac{3}{8}Q_{22}+Q_{66}\right)\right]_k \cdot\left(z_k - z_{k-1}\right)$$

$$\bar{A}_{66} = 2\pi R_X \sum_{k=1}^{n}\left[s_z^2 c_z^2\left(Q_{11}+\frac{3}{8}Q_{22}-Q_{12}-Q_{66}\right)+\frac{1}{2}\left(s_z^4+c_z^4\right)Q_{66}\right]_k \cdot\left(z_k - z_{k-1}\right)$$

$$\bar{B}_{11} = \pi R_X \sum_{k=1}^{n}\left[c_z^4 Q_{11} + s_z^2 c_z^2\left(Q_{12}+2Q_{66}\right)+\frac{3}{8}s_z^4 Q_{22}\right]_k \cdot\left(z_k^2 - z_{k-1}^2\right)$$

$$\bar{B}_{12} = \pi R_X \sum_{k=1}^{n}\left[s_z^2 c_z^2\left(Q_{11}+\frac{3}{8}Q_{22}-2Q_{66}\right)+\frac{1}{2}\left(s_z^4+c_z^4\right)Q_{66}\right]_k \cdot\left(z_k^2 - z_{k-1}^2\right)$$

$$\bar{B}_{22} = \pi R_X \sum_{k=1}^{n}\left[s_z^4 Q_{11} + s_z^2 c_z^2\left(Q_{12}+2Q_{66}\right)+\frac{3}{8}c_z^4 Q_{66}\right]_k \cdot\left(z_k^2 - z_{k-1}^2\right)$$

$$\bar{B}_{16} = \pi R_X \sum_{k=1}^{n}\left[s_z^3 c_z\left(Q_{11}-\frac{1}{2}Q_{12}-Q_{66}\right)+s_z c_z^3\left(\frac{1}{2}Q_{12}-\frac{3}{8}Q_{22}+Q_{66}\right)\right]_k \cdot\left(z_k^2 - z_{k-1}^2\right)$$

$$\bar{B}_{26} = 2\pi R_X \sum_{k=1}^{n}\left[c_z s_z^3\left(Q_{11}-\frac{1}{2}Q_{12}-Q_{66}\right)+c_z^3 s_z\left(\frac{1}{2}Q_{12}-\frac{3}{8}Q_{22}+Q_{66}\right)\right]_k \cdot\left(z_k^2 - z_{k-1}^2\right)$$

$$\bar{B}_{66} = 2\pi R_X \sum_{k=1}^{n}\left[s_z^2 c_z^2\left(Q_{11}+\frac{3}{8}Q_{22}-Q_{12}-Q_{66}\right)+\frac{1}{2}\left(s_z^4+c_z^4\right)Q_{66}\right]_k \cdot\left(z_k^2 - z_{k-1}^2\right)$$

$$\bar{D}_{11} = \frac{2\pi R_X}{3}\sum_{k=1}^{n}\left[c_z^4 Q_{11} + s_z^2 c_z^2\left(Q_{12}+2Q_{66}\right)+\frac{3}{8}s_z^4 Q_{22}\right]_k \cdot\left(z_k^3 - z_{k-1}^3\right)$$

$$+ 2\pi R_X^3 \sum_{k=1}^{n}\left[\frac{1}{2}c_z^4 Q_{11} + \frac{3}{4}s_z^2 c_z^2\left(Q_{12}+2Q_{66}\right)+\frac{5}{16}s_z^4 Q_{22}\right]_k \cdot\left(z_k - z_{k-1}\right)$$

$$\bar{D}_{12} = \frac{2\pi R_X}{3}\sum_{k=1}^{n}\left[s_z^2 c_z^2\left(Q_{11}+\frac{3}{8}Q_{22}-2Q_{66}\right)+\frac{1}{2}\left(s_z^4+c_z^4\right)Q_{66}\right]_k \cdot\left(z_k^3 - z_{k-1}^3\right)$$

$$+ 2\pi R_X^3 \sum_{k=1}^{n}\left[s_z^2 c_z^2\left(\frac{1}{2}Q_{11}+\frac{5}{16}Q_{22}-\frac{3}{2}Q_{66}\right)+\frac{3}{8}\left(s_z^4+c_z^4\right)Q_{12}\right]_k \cdot\left(z_k - z_{k-1}\right)$$

$$\bar{D}_{22} = \frac{2\pi R_X}{3}\sum_{k=1}^{n}\left[s_z^4 Q_{11} + s_z^2 c_z^2\left(Q_{12} + 2Q_{66}\right) + \frac{3}{8}c_z^4 Q_{22}\right]_k \cdot \left(z_k^3 - z_{k-1}^3\right)$$

$$+ 2\pi R_X^3 \sum_{k=1}^{n}\left[\frac{1}{2}s_z^4 Q_{11} + \frac{3}{4}s_z^2 c_z^2\left(Q_{12} + 2Q_{66}\right) + \frac{5}{16}c_z^4 Q_{22}\right]_k \cdot \left(z_k - z_{k-1}\right)$$

$$\bar{D}_{16} = \frac{2\pi R_X}{3}\sum_{k=1}^{n}\left[s_z^3 c_z\left(Q_{11} - \frac{1}{2}Q_{12} - Q_{66}\right) + s_z c_z^3\left(\frac{1}{2}Q_{12} - \frac{3}{8}Q_{22} + Q_{66}\right)\right]_k \cdot \left(z_k^3 - z_{k-1}^3\right)$$

$$+ 2\pi R_X^3 \sum_{k=1}^{n}\left[s_z c_z^3\left(\frac{1}{2}Q_{11} - \frac{3}{8}Q_{12} - \frac{3}{4}Q_{66}\right) + s_z^3 c_z\left(\frac{3}{8}Q_{12} - \frac{5}{16}Q_{22} + \frac{3}{4}Q_{66}\right)\right]_k \cdot \left(z_k - z_{k-1}\right)$$

$$\bar{D}_{26} = \frac{2\pi R_X}{3}\sum_{k=1}^{n}\left[s_z^3 c_z\left(Q_{11} - \frac{1}{2}Q_{12} - Q_{66}\right) + s_z c_z^3\left(\frac{1}{2}Q_{12} - \frac{3}{8}Q_{22} + Q_{66}\right)\right]_k \cdot \left(z_k^3 - z_{k-1}^3\right)$$

$$+ 2\pi R_X^3 \sum_{k=1}^{n}\left[s_z^3 c_z\left(\frac{1}{2}Q_{11} - \frac{3}{8}Q_{12} - \frac{3}{4}Q_{66}\right) + s_z c_z^3\left(\frac{3}{8}Q_{12} - \frac{5}{16}Q_{22} + \frac{3}{4}Q_{66}\right)\right]_k \cdot \left(z_k - z_{k-1}\right)$$

$$\bar{D}_{66} = \frac{2\pi R_X}{3}\sum_{k=1}^{n}\left[s_z^2 c_z^2\left(Q_{11} + \frac{3}{8}Q_{22} - Q_{12} - Q_{66}\right) + \frac{1}{2}\left(s_z^4 + c_z^4\right)Q_{66}\right]_k \cdot \left(z_k^3 - z_{k-1}^3\right)$$

$$+ 2\pi R_X^3 \sum_{k=1}^{n}\left[s_z^2 c_z^2\left(\frac{1}{2}Q_{11} + \frac{5}{16}Q_{22} - \frac{3}{4}Q_{12}\,\frac{3}{4}Q_{66}\right) + \frac{3}{8}\left(s_z^4 + c_z^4\right)Q_{66}\right]_k \cdot \left(z_k - z_{k-1}\right)$$

APPENDIX B

MATHEMATICA CODE FOR THE ANALYTICAL SOLUTION OF AXIAL DEFORMATION OF AN ISOTROPIC TUBE

```
Off[General::spell]
```

$$\text{tanalpha} = \frac{R_L - R_S}{L};$$

$$R_X = R_S + (L - x)\ \text{tanalpha};$$

$$A_X = \pi\left(\left(R_X + \frac{t}{2}\right)^2 - \left(R_X - \frac{t}{2}\right)^2\right);$$

$$\text{Def} = \left(\frac{F}{Y}\int \frac{dx}{A_X}\right)$$

$$-\frac{F\,L\,\text{Log}[2\,\pi\,t\,((L-x)\,R_L + x\,R_S)]}{2\,\pi\,t\,Y\,(R_L - R_S)}$$

$$\text{v1} = \text{Def} /. \{R_L \to 0.765,\ R_S \to 0.265,\ L \to 10,\ t \to 0.03,\ F \to 500,\ Y \to 1.0498\ 10^7\};$$

$$\text{v2} = \text{Table}\left[\frac{(\text{v1} /. x \to i) - (\text{v1} /. x \to 0)}{500}, \{i, 10\}\right] // \text{ColumnForm}$$

APPENDIX C

MATHEMATICA CODE FOR THE ANALYTICAL SOLUTION OF ANGLE OF TWIST OF AN ISOTROPIC TUBE

$t = 0.030;\ R_S = 0.265;\ R = 0.765;$

$L = 10;$

$$tanaplha = \frac{R - R_S}{L};$$

$T = 280;\ Y = 10.498\,10^6;\ \nu = 0.33;$

$$G = \frac{Y}{2(1+\nu)};$$

(*Rx=R- x tanaplha;*)

$$\phi = \frac{T}{\pi\, G\, t^3\, tanaplha}\ Log\left[\frac{R^2\,(t^2 + 4\,(R - x\,tanaplha)^2)}{(t^2 + 4\,R^2)\,(R - x\,tanaplha)^2}\right] /. x \to 10$$

APPENDIX D

MATHEMATICA CODE FOR THE ANALYTICAL SOLUTION OF AXIAL DEFORMATION AND ANGLE OF TWIST OF A TAPERED COMPOSITE TUBE

```
(* Closed form solution for stiffness of composite tube*)
Off[General::spell]
E1 = 22.8 10^6; E2 = 1.35 10^6; G12 = 0.83 10^6; ν12 = 0.3; t_ply = 0.005;
ν21 = E2 ν12 / E1;
(* Reduced Stiffness matrix of angle plies*)
Q11 = E1 / (1 - ν12 ν21); Q22 = E2 / (1 - ν12 ν21); Q12 = Q21 = E2 ν12 / (1 - ν12 ν21); Q66 = G12;
Q_1-2 = {{Q11, Q12, 0}, {Q21, Q22, 0}, {0, 0, Q66}};
R = 0.765; R_S = 0.265; L = 10; F = 500;

(*Transformation about X axis*)
mx = Cos[α];
tsigma = {{1, 0, 0}, {0, (mx)^2, 0}, {0, 0, mx}};
tepsilon = {{1, 0, 0}, {0, (mx)^2, 0}, {0, 0, mx}};
(Qbar_x-y,1 = Qbar_x-y,4 = tsigma.Q_1-2.tepsilon) // MatrixForm;
(Qbar_x-y,2 = Qbar_x-y,5 = tsigma.Q_1-2.tepsilon) // MatrixForm;
(Qbar_x-y,3 = Qbar_x-y,6 = tsigma.Q_1-2.tepsilon) // MatrixForm;

(*Transformation about Z axis*)
m[θ_] := Cos[θ]; n[θ_] := Sin[θ]
T_σ[θ_] := {{m[θ]^2, n[θ]^2, 2 m[θ] n[θ]}, {n[θ]^2, m[θ]^2, -2 m[θ] n[θ]},
  {-m[θ] n[θ], m[θ] n[θ], m[θ]^2 - n[θ]^2}}
T_ε[θ_] := {{m[θ]^2, n[θ]^2, m[θ] n[θ]}, {n[θ]^2, m[θ]^2, -m[θ] n[θ]},
  {-2 m[θ] n[θ], 2 m[θ] n[θ], m[θ]^2 - n[θ]^2}}
(Q_x-y,1 = Q_x-y,4 = T_σ[-θ].Qbar_x-y,1.T_ε[θ] /. θ → π/4) // MatrixForm;
(Q_x-y,2 = Q_x-y,5 = T_σ[-θ].Qbar_x-y,2.T_ε[θ] /. θ → -π/4) // MatrixForm;
(Q_x-y,3 = Q_x-y,6 = T_σ[-θ].Qbar_x-y,3.T_ε[θ] /. θ → 0) // MatrixForm;


tanphi = (R - R_S) / L;
R_X = R - (x tanphi); T = 280;

(* Distance from Mid planes*)
h = Table[i, {i, -3, 3}] t_ply;

(* A B D matrices *)
(A = Sum_{k=1}^{6} Q_x-y,k (h[[k + 1]] - h[[k]]) // Chop) // MatrixForm;
(B = 1/2 Sum_{k=1}^{6} Q_x-y,k (h[[k + 1]]^2 - h[[k]]^2) // Chop) // MatrixForm;
```

$$\left(D_{bs} = \frac{1}{3}\sum_{k=1}^{6} Q_{x\text{-}y,k}\left(h[[k+1]]^3 - h[[k]]^3\right) \text{ // Chop}\right) \text{ // MatrixForm;}$$

$$Ad = A;$$

$$Bd = B + R_X \text{Cos}[\alpha]\, A;$$

$$Dd = D_{bs} + 2\, R_X \text{Cos}[\alpha]\, B + (R_X)^2 (\text{Cos}[\alpha])^2 A;$$

$$\bar{A} = R_X \int_0^{2\pi} Ad\, d\alpha \text{ // Chop;}$$

$$\left(\bar{B} = R_X \int_0^{2\pi} Bd\, d\alpha\right) \text{ // Chop // MatrixForm;}$$

$$\bar{D} = R_X \int_0^{2\pi} Dd\, d\alpha \text{ // Chop;}$$

$$\left(a = \text{Inverse}[\bar{A}] \text{ // Simplify}\right) \text{ // MatrixForm}$$

$$\delta = F \int_0^{10} a[[1, 1]]\, dx$$

$$\left(*\delta = \frac{F\, a[[1,1]]}{\text{tanalpha}}\ \text{Log}\left[\frac{R}{R - x\ \text{tanalpha}}\right] /. x \to 10 *\right)$$

$$d = \text{Inverse}[\bar{D}];$$

$$u = \text{Apart}[d[[3, 3]]];$$

$$\phi = \text{TChop}[\text{Sum}[\text{Integrate}[u[[i]], \{x, 0, 10\}], \{i, \text{Length}[u]\}]]$$

APPENDIX E

ANSYS BATCH FILE FOR THE GENERATION OF THE FINITE ELEMENT MODEL

```
!* COMPOSITE TAPERED TUBE MADE OF 1M6/3501-6 WITH LAY-UP [45/-45/0]S

/PREP7
!*
MP,EX,1,22.8E6
MP,EY,1,1.35E6
MP,EZ,1,1.35E6
MP,PRXY,1,0.3
MP,PRYZ,1,0.3
MP,PRXZ,1,0.3
MP,GXY,1,0.83E6
MP,GYZ,1,0.83E6
MP,GXZ,1,0.83E6
!*
ET,1,SOLID46
!*
KEYOPT,1,2,0
KEYOPT,1,1,0
KEYOPT,1,3,0
KEYOPT,1,4,0
KEYOPT,1,5,0
KEYOPT,1,6,0
KEYOPT,1,8,1
KEYOPT,1,9,0
KEYOPT,1,10,0
!*
!* LAYER 1
R,1
RMODIF,1,1,1,0,0,0
RMODIF,1,7,0
!*
RMODIF,1,13,1,45,0.005
!*
!* LAYER 2
R,2
RMODIF,2,1,1,0,0,0
RMODIF,2,7,0
!*
RMODIF,2,13,1,-45,0.005
!*
!* LAYER 3
R,3
RMODIF,3,1,1,0,0,0
RMODIF,3,7,0
!*
RMODIF,3,13,1,0,0.005
```

```
!*
!* LAYER 4
R,4
RMODIF,4,1,1,0,0,0
RMODIF,4,7,0
!*
RMODIF,4,13,1,45,0.005
!*
!* LAYER 5
R,5
RMODIF,5,1,1,0,0,0
RMODIF,5,7,0
!*
RMODIF,5,13,1,-45,0.005
!*
!* LAYER 6
R,6
RMODIF,6,1,1,0,0,0
RMODIF,6,7,0
!*
RMODIF,6,13,1,0,0.005
!*
!*
ET,2,MASS21
!*
!*
KEYOPT,1,1,0
KEYOPT,1,2,0
KEYOPT,1,3,0
!*
!*
R,7,1,1,1, , , ,
!*
!*CREATING KEYPOINTS
!*
*DO,I,1,7,1

K,I*10+1,0,0.75+(I-1)*0.005,0
K,I*10+2,10,0.25+(I-1)*0.005,0

*ENDDO
!*
!*CREATING AREAS USING KEYPOINTS
!*
*DO,I,1,6,1
```

```
A,11+(I-1)*10,12+(I-1)*10,12+(I*10),11+(I*10)

*ENDDO

AGLUE,ALL

K,13,0,0,0
K,14,10,0,0
!*
!* ROTATE AREAS TO FORM VOLUMES
!*
VROTAT,ALL,,,,,,13,14,,2

VGLUE,ALL
!*
!* CHANGING ATTRIBUTES OF VOLUMES TO LAYER PROPERTIES
*DO,K,1,6,1

        VSEL,S,VOLU,,K
        VATT,1,K,1,0
*ENDDO

*DO,K,1,6,1

        VSEL,S,VOLU,,K+6
        VATT,1,K,1,0
*ENDDO
!*
!*DEFINING ELEMENT SIZES FOR LINES
!*
LSEL,S,LENGTH,,0.005,,,0
LESIZE,ALL,,,1
CM,THICKNESSLINE,LINE

LSEL,S,LENGTH,,10.012,,,0
LESIZE,ALL,,,40
CM,LENGTHLINE,LINE

ALLSEL,ALL,LINE
LSEL,U,LENGTH,,0.005,,,0
LSEL,U,LENGTH,,10.012,,,0
LESIZE,ALL,,,12
!*
!* CREATING NODES ON KEYPOINTS 13 AND 14
!*
NKPT,,13
```

```
NKPT,,14
!*
!* CREATING A MASS21 ELEMENT FOR MASTER NODE
!*
TYPE,2
REAL,7
E,2
!*
!* MESHING THE VOLUMES
!*
VSEL,S,VOLU,,ALL
VPLOT
VMESH,ALL
```

REFERENCES

[1] Reddy, J N. (2003). Mechanics of Laminated composite plates and shells - Theory and Analysis. CRC Press.

[2] Chan, W. S. and Demirhan, K. C., (1997). "A Simple Closed-Form Solution of Bending Stiffness for Laminated Composite Tubes", Journal of reinforced plastics and composites, Volume 19, Issue 4, 2000, Pages 278-291

[3] Lin, C.Y. and Chan, W.S., (2003). "A simple analytical method for analyzing laminated composite elliptical tubes", Proceedings of 17th technical conference, American Society of composites, October 2002.

[4] Ren, J. G. (1995). "Analysis of laminated circular cylindrical shells under axisymmetric loading", Composite Structures, Volume 30, Issue 3, 1995, Pages 271-280

[5] Tafreshi, A. and Bailey, C.G., (2007). "Instability of imperfect composite cylindrical shells under combined loading", Composite Structures, Volume 80, Issue 1, September 2007, Pages 49-64

[6] Vaziri, A., (2007). “On the buckling of cracked composite cylindrical shells under axial compression”, Composite Structures, Volume 80, Issue 1, September 2007, Pages 152-158

[7] Yan, W., Ying, J. and Chen, W.Q.,(2007). “The behavior of angle-ply laminated cylindrical shells with viscoelastic interfaces in cylindrical bending”, Composite Structures, Volume 78, Issue 4, June 2007, Pages 551-559

[8] Gummadi, L. N. B. and Palazotto, A.N., (1998). “Progressive failure analysis of composite cylindrical shells considering large rotations”, Composites Part B, Volume 29, Issue 5, September 1998, Pages 547-563

[9] Correia, P. I. F., Soares, M. C.M. and Herskovits, J (2003). “Analysis of Laminated Conical Shell Structures Using Higher Order Models”, Composite Structures, Volume 62, Issue 3, 2003, Pages. 383-390

[10] Liu, R.H (1996). “Non Linear Buckling of Symmetrically Laminated, Cylindrically Orthotropic, Shallow Conical Shells considering Shear”, International Journal of Non-Linear Mechanics, Volume 31, Issue 1, January 1996, Pages 89-99

[11] Goldfield, Y., (2007). “Elastic buckling and imperfection sensitivity of generally stiffened conical shells”, AIAA Journal, Volume 45, Issue 3, March 2007

[12] Raju, B. B., Chandra, R. and Subba Rao, M., (1978). "Transient Temperatures in Laminated Composite Conical shells due to Aerodynamic Heating", AIAA Journal, Volume 16, Number 6, 1978

[13] Ghosh, A. and Sinha, P. K., (2005). "Initiation and propogation of damage in laminated composite shells due to low velocity impact", International Journal of Crashworthiness, Volume 10, Issue 4, Pages 379-388

[14] Mahdi, E., Hamouda, A.M.S., Sahari, B.B. and Khalid, Y.A., (2002). "Effect of Material and Geometry on Crushing Behavior of Laminated Conical Composite Shells", Applied Composite Materials, Volume 9, Issue 5, September 2002, Pages 265-290

[15] Movsumov, E. A., and Shamiev, F. H. (2006). "Yield Condition for Circular Cylindrical Shells Made of a Fiber Reinforced Composite", Mechanics of Composite Materials, Volume 42, Issue 5, September 2006, Pages 459-466

[16] Naidu, N.V.S. and Sinha, P.K. (2005). "Nonlinear finite element analysis of laminated composite shells in hygrothermal environments", Composite Structures, Volume 69, Issue 4, August 2005, Pages 387-395

[17] Tafreshi, A., (2004). "Efficient modeling of delamination buckling in composite cylindrical shells under axial compression", Composite Structures, Volume 64, Issues 3-4, June 2004, Pages 511-520

[18] Bhimaraddi, A. and Chandrashekhara, K., (1992). "Three-dimensional elasticity solution for static response of simply supported orthotropic cylindrical shells", Composite Structures, Volume 20, Issue 4, 1992, Pages 227-235

[19] Saggar, P. (2007). Experimental Study of Laminated Composite Tubes under Bending, Master's Thesis, University of Texas at Arlington, May 2007

BIOGRAPHICAL INFORMATION

Chethana Shankara Rao received her Bachelor's degree from Visveswaraiah Technological University, India in 2003. She began her Master's program in Mechanical engineering at U.T. Arlington from August 2004.

Her research interests include Stress analysis, structural dynamics, fracture mechanics and composite materials. She has carried out various projects on structural analysis and intends to work in this field soon after the master's degree. She also intends to pursue a PhD degree in the future.

Chethana Shankara Rao received her master's degree in mechanical engineering from U.T Arlington in May 2007.